

Sklar, B. "Rayleigh Fading Channels"  
*Mobile Communications Handbook*  
Ed. Suthan S. Suthersan  
Boca Raton: CRC Press LLC, 1999

# Rayleigh Fading Channels<sup>1</sup>

---

- 18.1 Introduction
- 18.2 The Challenge of a Fading Channel
- 18.3 Mobile-Radio Propagation: Large-Scale Fading and Small-Scale Fading
  - Large-Scale Fading: Path-Loss Mean and Standard Deviation
  - Small-Scale Fading: Statistics and Mechanisms
- 18.4 Signal Time-Spreading Viewed in the Time-Delay Domain: Figure 18.1, Block 7—The Multipath Intensity Profile
  - Degradation Categories due to Signal Time-Spreading Viewed in the Time Delay Domain
- 18.5 Signal Time-Spreading Viewed in the Frequency Domain: Figure 18.1, Block 10—The Spaced-Frequency Correlation Function
  - Degradation Categories due to Signal Time-Spreading Viewed in the Frequency Domain
- 18.6 Typical Examples of Flat Fading and Frequency-Selective Fading Manifestations
- 18.7 Time Variance Viewed in the Time Domain: Figure 18.1, Block 13—The Spaced-Time Correlation Function
  - The Concept of Duality • Degradation Categories due to Time Variance Viewed in the Time Domain
- 18.8 Time Variance Viewed in the Doppler-Shift Domain: Figure 18.1, Block 16—The Doppler Power Spectrum
- 18.9 Analogy Between Spectral Broadening in Fading Channels and Spectral Broadening in Digital Signal Keying
- 18.10 Degradation Categories due to Time Variance, Viewed in the Doppler-Shift Domain
- 18.11 Mitigation Methods
  - Mitigation to Combat Frequency-Selective Distortion • Mitigation to Combat Fast-Fading Distortion • Mitigation to Combat Loss in SNR
- 18.12 Summary of the Key Parameters Characterizing Fading Channels
  - Fast-Fading Distortion: Example #1 • Frequency-Selective Fading Distortion: Example #2 • Fast-Fading and Frequency-Selective Fading Distortion: Example #3
- 18.13 The Viterbi Equalizer as Applied to GSM
- 18.14 The Rake Receiver Applied to Direct-Sequence Spread-Spectrum (DS/SS) Systems
- 18.15 Conclusion
- References

Bernard Sklar  
*Communications Engineering Services*

## 18.1 Introduction

---

When the mechanisms of fading channels were first modeled in the 1950s and 1960s, the ideas were primarily applied to over-the-horizon communications covering a wide range of frequency bands. The 3–30 MHz high-frequency (HF) band is used for ionospheric communications, and the 300 MHz–3 GHz ultra-high-frequency (UHF) and 3–30 GHz super-high-frequency (SHF) bands are used for tropospheric scatter. Although the fading effects in a mobile radio system are somewhat different from those in ionospheric and tropospheric channels, the early models are still quite useful to help characterize fading effects in mobile digital communication systems. This chapter addresses Rayleigh fading, primarily in the UHF band, that affects mobile systems such as cellular and personal communication systems (PCS). The chapter itemizes the fundamental fading manifestations, types of degradation, and methods to mitigate the degradation. Two particular mitigation techniques are examined: the Viterbi equalizer implemented in the Global System for Mobile Communication (GSM), and the Rake receiver used in CDMA systems built to meet Interim Standard-95 (IS-95).

## 18.2 The Challenge of a Fading Channel

---

In the study of communication systems, the classical (ideal) additive-white-Gaussian-noise (AWGN) channel, with statistically independent Gaussian noise samples corrupting data samples free of intersymbol interference (ISI), is the usual starting point for understanding basic performance relationships. The primary source of performance degradation is thermal noise generated in the receiver. Often, external interference received by the antenna is more significant than the thermal noise. This external interference can sometimes be characterized as having a broadband spectrum and quantified by a parameter called antenna temperature [1]. The thermal noise usually has a flat power spectral density over the signal band and a zero-mean Gaussian voltage probability density function (pdf). When modeling practical systems, the next step is the introduction of bandlimiting filters. The filter in the transmitter usually serves to satisfy some regulatory requirement on spectral containment. The filter in the receiver often serves the purpose of a classical “matched filter” [2] to the signal bandwidth. Due to the bandlimiting and phase-distortion properties of filters, special signal design and equalization techniques may be required to mitigate the filter-induced ISI.

If a radio channel’s propagating characteristics are not specified, one usually infers that the signal attenuation vs. distance behaves as if propagation takes place over ideal free space. The model of free space treats the region between the transmit and receive antennas as being free of all objects that might absorb or reflect radio frequency (RF) energy. It also assumes that, within this region, the atmosphere behaves as a perfectly uniform and nonabsorbing medium. Furthermore, the earth is treated as being infinitely far away from the propagating signal (or, equivalently, as having a reflection coefficient that is negligible). Basically, in this idealized free-space model, the attenuation of RF energy between the transmitter and receiver behaves according to an inverse-square law. The received power expressed in terms of transmitted power is attenuated by a factor,  $L_s(d)$ , where this factor is called **path loss** or

---

<sup>1</sup>A version of this chapter has appeared as two papers in the *IEEE Communications Magazine*, September 1997, under the titles “Rayleigh Fading Channels in Mobile Digital Communication Systems, Part I: Characterization” and “Part II: Mitigation.”

**free space loss.** When the receiving antenna is isotropic, this factor is expressed as [1]:

$$L_s(d) = \left( \frac{4\pi d}{\lambda} \right)^2 \quad (18.1)$$

In Eq. (18.1),  $d$  is the distance between the transmitter and the receiver, and  $\lambda$  is the wavelength of the propagating signal. For this case of idealized propagation, received signal power is very predictable.

For most practical channels, where signal propagation takes place in the atmosphere and near the ground, the free-space propagation model is inadequate to describe the channel and predict system performance. In a wireless mobile communication system, a signal can travel from transmitter to receiver over multiple reflective paths; this phenomenon is referred to as **multipath propagation**. The effect can cause fluctuations in the received signal's amplitude, phase, and angle of arrival, giving rise to the terminology **multipath fading**. Another name, **scintillation**, having originated in radio astronomy, is used to describe the multipath fading caused by physical changes in the propagating medium, such as variations in the density of ions in the ionospheric layers that reflect high frequency (HF) radio signals. Both names, fading and scintillation, refer to a signal's random fluctuations or fading due to multipath propagation. The main difference is that scintillation involves mechanisms (e.g., ions) that are much smaller than a wavelength. The end-to-end modeling and design of systems that mitigate the effects of fading are usually more challenging than those whose sole source of performance degradation is AWGN.

### 18.3 Mobile-Radio Propagation: Large-Scale Fading and Small-Scale Fading

---

Figure 18.1 represents an overview of fading channel manifestations. It starts with two types of fading effects that characterize mobile communications: large-scale fading and small-scale fading. Large-scale fading represents the average signal power attenuation or the path loss due to motion over large areas. In Fig. 18.1, the large-scale fading manifestation is shown in blocks 1, 2, and 3. This phenomenon is affected by prominent terrain contours (e.g., hills, forests, billboards, clumps of buildings, etc.) between the transmitter and receiver. The receiver is often represented as being “shadowed” by such prominences. The statistics of large-scale fading provide a way of computing an estimate of path loss as a function of distance. This is described in terms of a mean-path loss ( $n$ th-power law) and a log-normally distributed variation about the mean. Small-scale fading refers to the dramatic changes in signal amplitude and phase that can be experienced as a result of small changes (as small as a half-wavelength) in the spatial separation between a receiver and transmitter. As indicated in Fig. 18.1, blocks 4, 5, and 6, small-scale fading manifests itself in two mechanisms, namely, time-spreading of the signal (or signal dispersion) and time-variant behavior of the channel. For mobile-radio applications, the channel is time-variant because motion between the transmitter and receiver results in propagation path changes. The rate of change of these propagation conditions accounts for the fading rapidity (rate of change of the fading impairments). Small-scale fading is also called **Rayleigh fading** because if the multiple reflective paths are large in number and there is no line-of-sight signal component, the envelope of the received signal is statistically described by a Rayleigh pdf. When there is a dominant nonfading signal component present, such as a line-of-sight propagation path, the small-scale fading envelope is described by a Rician pdf [3]. A mobile radio roaming over a large area must process signals that experience both types of fading: small-scale fading superimposed on large-scale fading.

There are three basic mechanisms that impact signal propagation in a mobile communication system. They are reflection, diffraction, and scattering [3].

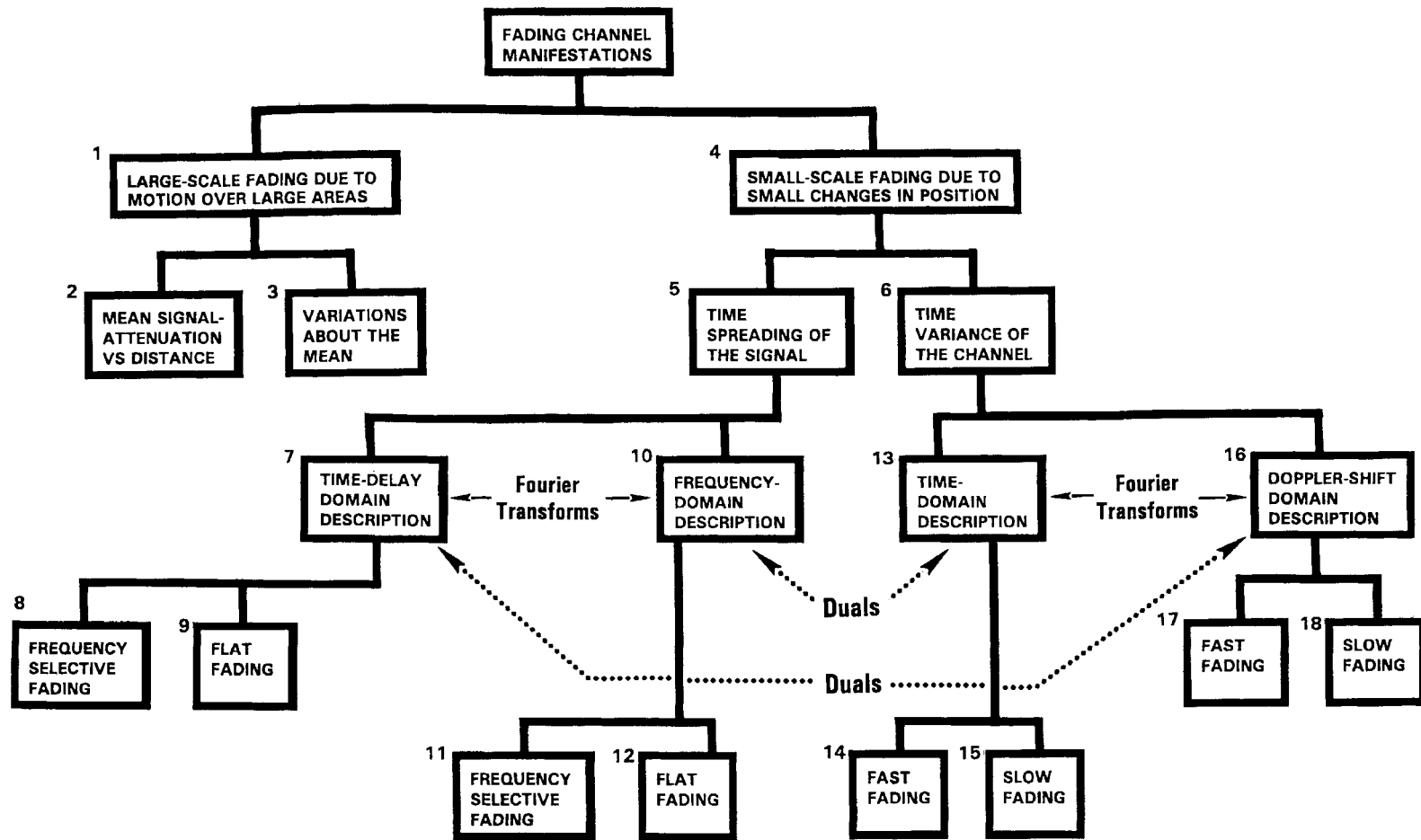


FIGURE 18.1: Fading channel manifestations.

- Reflection occurs when a propagating electromagnetic wave impinges upon a smooth surface with very large dimensions compared to the RF signal wavelength ( $\lambda$ ).
- Diffraction occurs when the radio path between the transmitter and receiver is obstructed by a dense body with large dimensions compared to  $\lambda$ , causing secondary waves to be formed behind the obstructing body. Diffraction is a phenomenon that accounts for RF energy travelling from transmitter to receiver without a line-of-sight path between the two. It is often termed **shadowing** because the diffracted field can reach the receiver even when shadowed by an impenetrable obstruction.
- Scattering occurs when a radio wave impinges on either a large rough surface or any surface whose dimensions are on the order of  $\lambda$  or less, causing the reflected energy to spread out (scatter) in all directions. In an urban environment, typical signal obstructions that yield scattering are lampposts, street signs, and foliage.

Figure 18.1 may serve as a table of contents for the sections that follow. We will examine the two manifestations of small-scale fading: signal time-spreading (signal dispersion) and the time-variant nature of the channel. These examinations will take place in two domains: time and frequency, as indicated in Fig. 18.1, blocks 7, 10, 13, and 16. For signal dispersion, we categorize the fading degradation types as being frequency-selective or frequency-nonselective (flat), as listed in blocks 8, 9, 11, and 12. For the time-variant manifestation, we categorize the fading degradation types as fast-fading or slow-fading, as listed in blocks 14, 15, 17, and 18. The labels indicating Fourier transforms and duals will be explained later.

Figure 18.2 illustrates the various contributions that must be considered when estimating path loss for a link budget analysis in a cellular application [4]. These contributions are:

- Mean path loss as a function of distance, due to large-scale fading
- Near-worst-case variations about the mean path loss (typically 6–10 dB) or large-scale fading margin
- Near-worst-case Rayleigh or small-scale fading margin (typically 20–30 dB)

In Fig. 18.2, the annotations “ $\approx 1\text{--}2\%$ ” indicate a suggested area (probability) under the tail of each pdf as a design goal. Hence, the amount of margin indicated is intended to provide adequate received signal power for approximately 98–99% of each type of fading variation (large- and small-scale).

A received signal, is generally described in terms of a transmitted signal  $s(t)$  convolved with the impulse response of the channel  $h_c(t)$ . Neglecting the degradation due to noise, we write:

$$r(t) = s(t) * h_c(t) \quad (18.2)$$

where  $*$  denotes convolution. In the case of mobile radios,  $r(t)$  can be partitioned in terms of two component random variables, as follows [5]:

$$r(t) = m(t) \times r_0(t) \quad (18.3)$$

where  $m(t)$  is called the large-scale-fading component, and  $r_0(t)$  is called the small-scale-fading component.  $m(t)$  is sometimes referred to as the **local mean** or **log-normal fading** because the magnitude of  $m(t)$  is described by a log-normal pdf (or, equivalently, the magnitude measured in decibels has a Gaussian pdf).  $r_0(t)$  is sometimes referred to as multipath or Rayleigh fading. Figure 18.3 illustrates the relationship between large-scale and small-scale fading. In Fig. 18.3(a), received signal power  $r(t)$  vs. antenna displacement (typically in units of wavelength) is plotted for the case of a mobile radio. Small-scale fading superimposed on large-scale fading can be readily

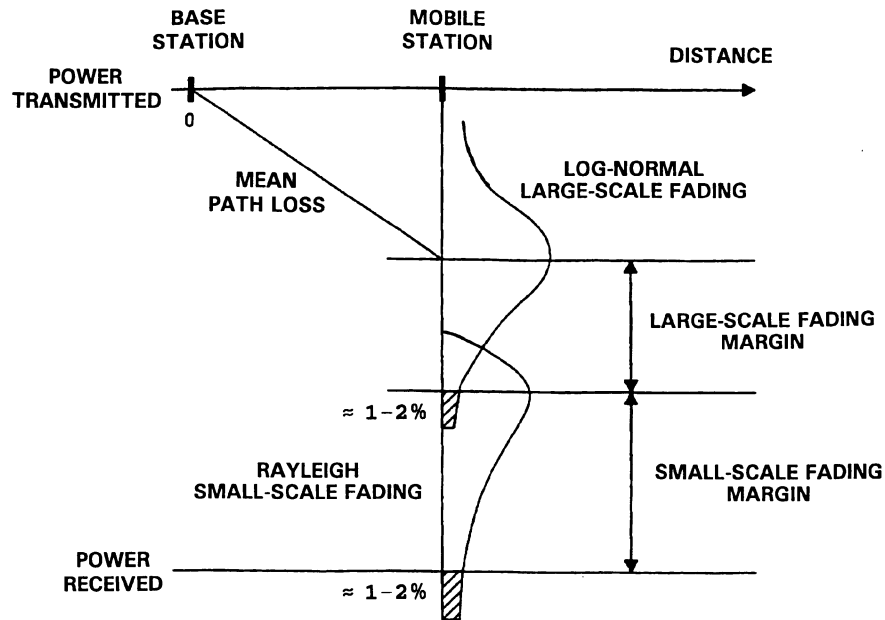


FIGURE 18.2: Link-budget considerations for a fading channel.

identified. The typical antenna displacement between the small-scale signal nulls is approximately a half wavelength. In Fig. 18.3(b), the large-scale fading or local mean,  $m(t)$ , has been removed in order to view the small-scale fading,  $r_0(t)$ , about some average constant power.

In the sections that follow, we enumerate some of the details regarding the statistics and mechanisms of large-scale and small-scale fading.

### 18.3.1 Large-Scale Fading: Path-Loss Mean and Standard Deviation

For the mobile radio application, Okumura [6] made some of the earlier comprehensive path-loss measurements for a wide range of antenna heights and coverage distances. Hata [7] transformed Okumura's data into parametric formulas. For the mobile radio application, the mean path loss,  $\overline{L}_p(d)$ , as a function of distance,  $d$ , between the transmitter and receiver is proportional to an  $n$ th-power of  $d$  relative to a reference distance  $d_0$  [3].

$$\overline{L}_p(d) \propto \left(\frac{d}{d_0}\right)^n \quad (18.4)$$

$\overline{L}_p(d)$  is often stated in decibels, as shown below.

$$\overline{L}_p(d) \text{ (dB)} = L_s(d_0) \text{ (dB)} + 10n \log\left(\frac{d}{d_0}\right) \quad (18.5)$$

The reference distance  $d_0$ , corresponds to a point located in the far field of the antenna. Typically, the value of  $d_0$  is taken to be 1 km for large cells, 100 m for microcells, and 1 m for indoor channels.  $\overline{L}_p(d)$  is the average path loss (over a multitude of different sites) for a given value of  $d$ . Linear

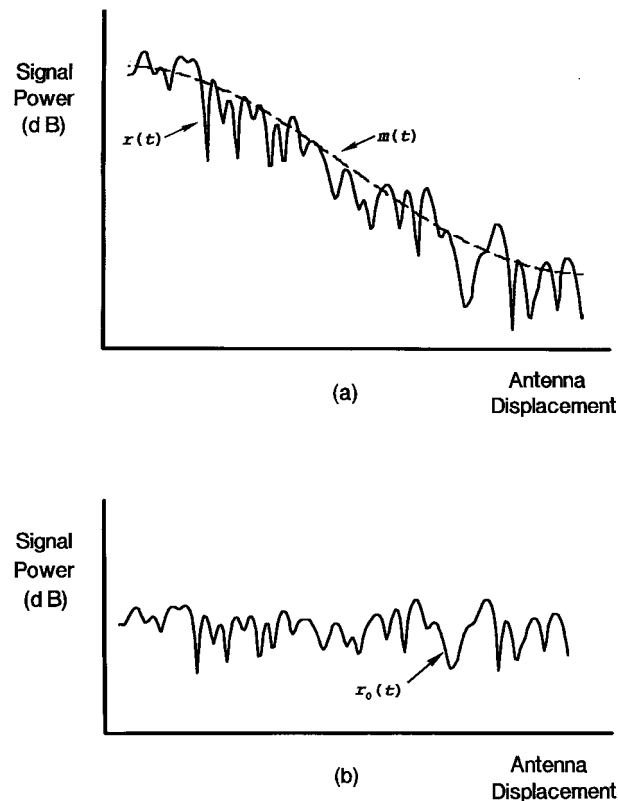


FIGURE 18.3: Large-scale fading and small-scale fading.

regression for a minimum mean-squared estimate (MMSE) fit of  $\overline{L_p}(d)$  vs.  $d$  on a log-log scale (for distances greater than  $d_0$ ) yields a straight line with a slope equal to  $10n$  dB/decade. The value of the exponent  $n$  depends on the frequency, antenna heights, and propagation environment. In free space,  $n = 2$ , as seen in Eq. (18.1). In the presence of a very strong guided wave phenomenon (like urban streets),  $n$  can be lower than 2. When obstructions are present,  $n$  is larger. The path loss  $L_s(d_0)$  to the reference point at a distance  $d_0$  from the transmitter is typically found through field measurements or is calculated using the free-space path loss given by Eq. (18.1). Figure 18.4 shows a scatter plot of path loss vs. distance for measurements made in several German cities [8]. Here, the path loss has been measured relative to the free-space reference measurement at  $d_0 = 100$  m. Also shown are straight-line fits to various exponent values.

The path loss vs. distance expressed in Eq. (18.5) is an average, and therefore not adequate to describe any particular setting or signal path. It is necessary to provide for variations about the mean since the environment of different sites may be quite different for similar transmitter-receiver separations. Figure 18.4 illustrates that path-loss variations can be quite large. Measurements have shown that for any value of  $d$ , the path loss  $L_p(d)$  is a random variable having a log-normal distribution about the mean distant-dependent value  $\overline{L_p}(d)$  [9]. Thus, path loss  $L_p(d)$  can be

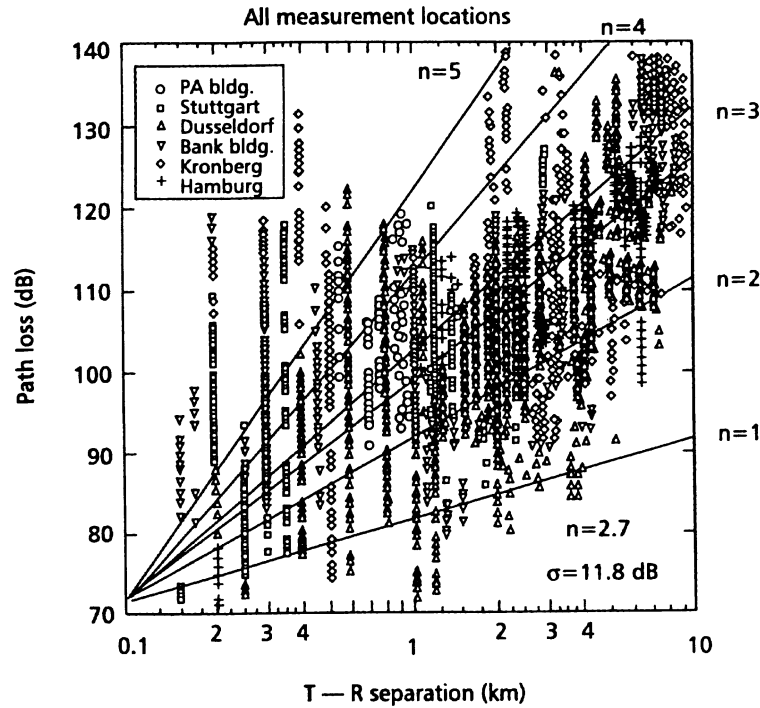


FIGURE 18.4: Path loss vs. distance measured in several German cities.

expressed in terms of  $\overline{L_p}(d)$  plus a random variable  $X_\sigma$ , as follows [3].

$$L_p(d) \text{ (dB)} = L_s(d_0) \text{ (dB)} + 10n \log_{10} \left( \frac{d}{d_0} \right) + X_\sigma \text{ (dB)} \quad (18.6)$$

where  $X_\sigma$  denotes a zero-mean, Gaussian random variable (in decibels) with standard deviation  $\sigma$  (also in decibels).  $X_\sigma$  is site and distance dependent. The choice of a value for  $X_\sigma$  is often based on measurements; it is not unusual for  $X_\sigma$  to take on values as high as 6–10 dB or greater. Thus, the parameters needed to statistically describe path loss due to large-scale fading for an arbitrary location with a specific transmitter-receiver separation are:

- The reference distance  $d_0$
- The path-loss exponent  $n$
- The standard deviation  $\sigma$  of  $X_\sigma$

There are several good references dealing with the measurement and estimation of propagation path loss for many different applications and configurations [3], [7]–[11].

### 18.3.2 Small-Scale Fading: Statistics and Mechanisms

When the received signal is made up of multiple reflective rays plus a significant line-of-sight (non-faded) component, the envelope amplitude due to small-scale fading has a Rician pdf, and is referred to as **Rician fading** [3]. The nonfaded component is called the **specular component**. As the amplitude of the specular component approaches zero, the Rician pdf approaches a Rayleigh pdf, expressed as:

$$p(r) = \begin{cases} \frac{r}{\sigma^2} \exp\left[-\frac{r^2}{2\sigma^2}\right] & \text{for } r \geq 0 \\ 0 & \text{otherwise} \end{cases} \quad (18.7)$$

where  $r$  is the envelope amplitude of the received signal, and  $2\sigma^2$  is the predetection mean power of the multipath signal. The Rayleigh faded component is sometimes called the **random, scatter, or diffuse component**. The Rayleigh pdf results from having no specular component of the signal; thus for a single link it represents the pdf associated with the worst case of fading per mean received signal power. For the remainder of this chapter, it will be assumed that loss of signal-to-noise ratio (SNR) due to fading follows the Rayleigh model described. It will also be assumed that the propagating signal is in the UHF band, encompassing present-day cellular and personal communications services (PCS) frequency allocations—nominally 1 GHz and 2 GHz, respectively.

As indicated in Fig. 18.1, blocks 4, 5, and 6, small-scale fading manifests itself in two mechanisms:

- Time-spreading of the underlying digital pulses within the signal
- A time-variant behavior of the channel due to motion (e.g., a receive antenna on a moving platform).

Figure 18.5 illustrates the consequences of both manifestations by showing the response of a multipath channel to a narrow pulse vs. delay, as a function of antenna position (or time, assuming a constant velocity of motion). In Fig. 18.5, we distinguish between two different time references—delay time  $\tau$  and transmission or observation time  $t$ . Delay time refers to the time-spreading manifestation which results from the fading channel's nonoptimum impulse response. The transmission time, however, is related to the antenna's motion or spatial changes, accounting for propagation path changes that are perceived as the channel's time-variant behavior. Note that, for constant velocity, as is assumed in Fig. 18.5, either antenna position or transmission time can be used to illustrate this time-variant behavior. Figures 18.5(a)–(c) show the sequence of received pulse-power profiles as the antenna moves through a succession of equally spaced positions. Here, the interval between antenna positions is  $0.4\lambda$ , where  $\lambda$  is the wavelength of the carrier frequency. For each of the three cases shown, the response-pattern differs significantly in the delay time of the largest signal component, the number of signal copies, their magnitudes, and the total received power (area) in the received power profile. Figure 18.6 summarizes these two small-scale fading mechanisms, the two domains (time or time-delay and frequency or Doppler shift) for viewing each mechanism and the degradation categories each mechanism can exhibit. Note that any mechanism characterized in the time domain can be characterized equally well in the frequency domain. Hence, as outlined in Fig. 18.6, the time-spreading mechanism will be characterized in the time-delay domain as a multipath delay spread and in the frequency domain as a channel coherence bandwidth. Similarly, the time-variant mechanism will be characterized in the time domain as a channel coherence time and in the Doppler-shift (frequency) domain as a channel fading rate or Doppler spread. These mechanisms and their associated degradation categories will be examined in greater detail in the sections that follow.

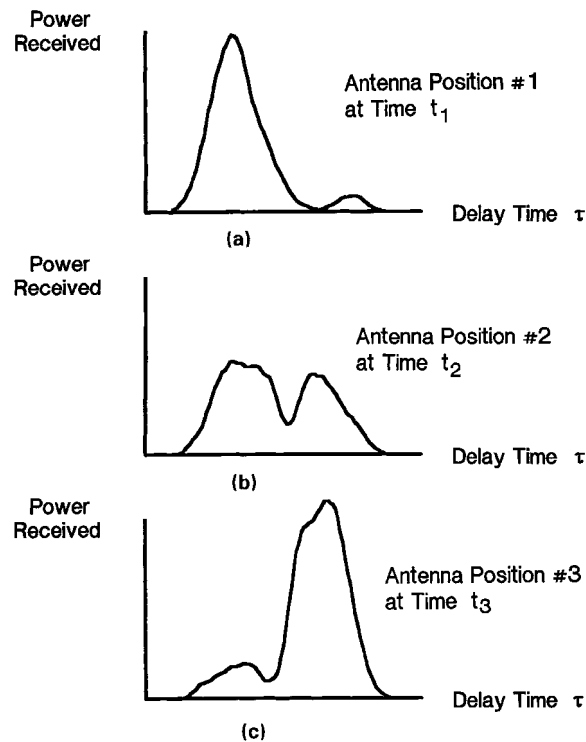


FIGURE 18.5: Response of a multipath channel to a narrow pulse vs. delay, as a function of antenna position.

## 18.4 Signal Time-Spreading Viewed in the Time-Delay Domain: Figure 18.1, Block 7—The Multipath Intensity Profile

A simple way to model the fading phenomenon was introduced by Bello [13] in 1963; he proposed the notion of wide-sense stationary uncorrelated scattering (WSSUS). The model treats signal variations arriving with different delays as uncorrelated. It can be shown [4, 13] that such a channel is effectively WSS in both the time and frequency domains. With such a model of a fading channel, Bello was able to define functions that apply for all time and all frequencies. For the mobile channel, Fig. 18.7 contains four functions that make up this model [4], [13]–[16]. We will examine these functions, starting with Fig. 18.7(a) and proceeding counter-clockwise toward Fig. 18.7(d).

In Fig. 18.7(a), a **multipath-intensity profile**,  $S(\tau)$  vs. time delay  $\tau$  is plotted. Knowledge of  $S(\tau)$  helps answer the question, “For a transmitted impulse, how does the average received power vary as a function of time delay,  $\tau$ ?” The term “time delay” is used to refer to the excess delay. It represents the signal’s propagation delay that exceeds the delay of the first signal arrival at the receiver. For a typical wireless radio channel, the received signal usually consists of several discrete multipath components, sometimes referred to as fingers. For some channels, such as the tropospheric scatter channel, received signals are often seen as a continuum of multipath components [14, 16]. For making measurements of the multipath intensity profile, wideband signals (impulses or spread

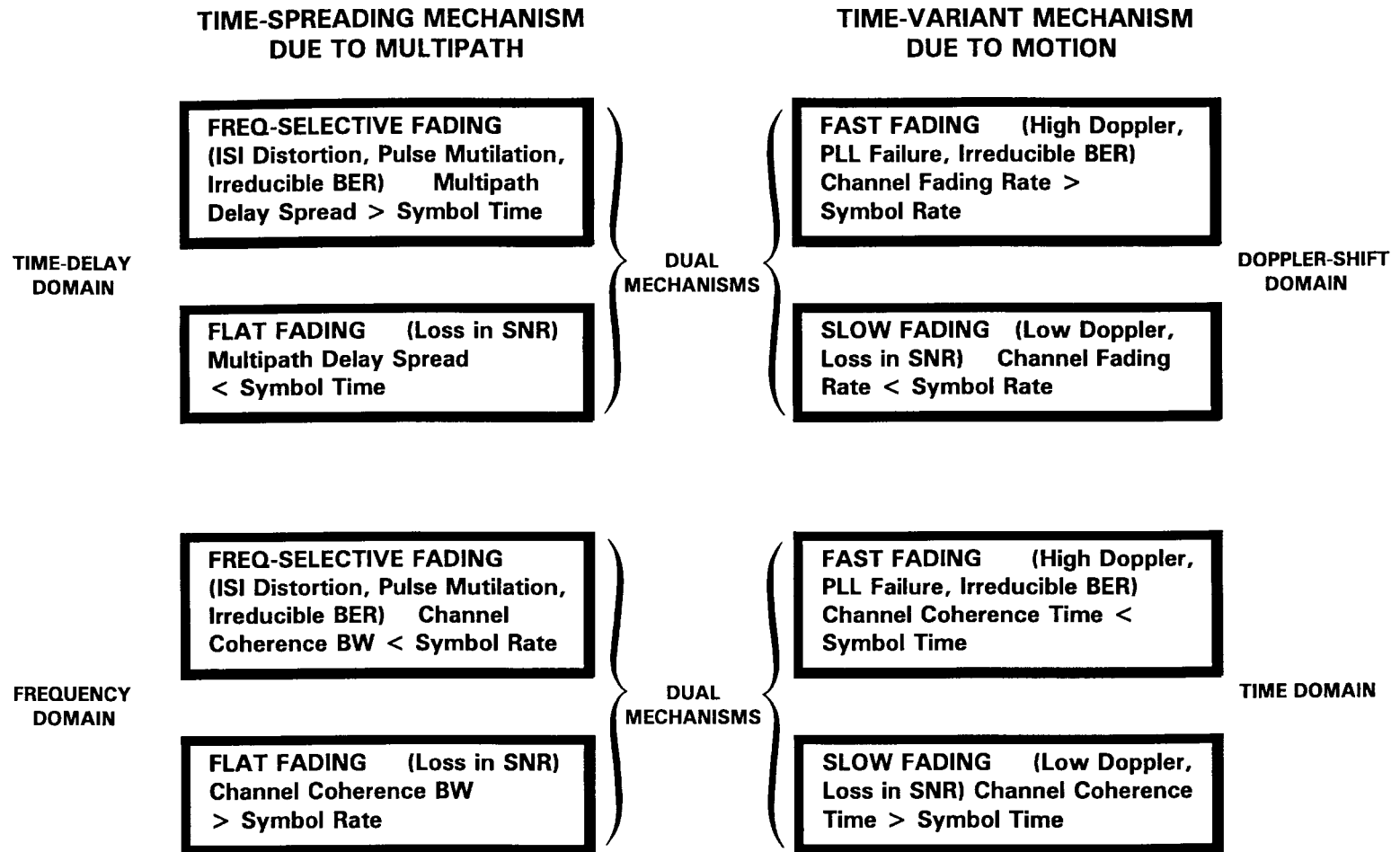


FIGURE 18.6: Small-scale fading: mechanisms, degradation categories, and effects.

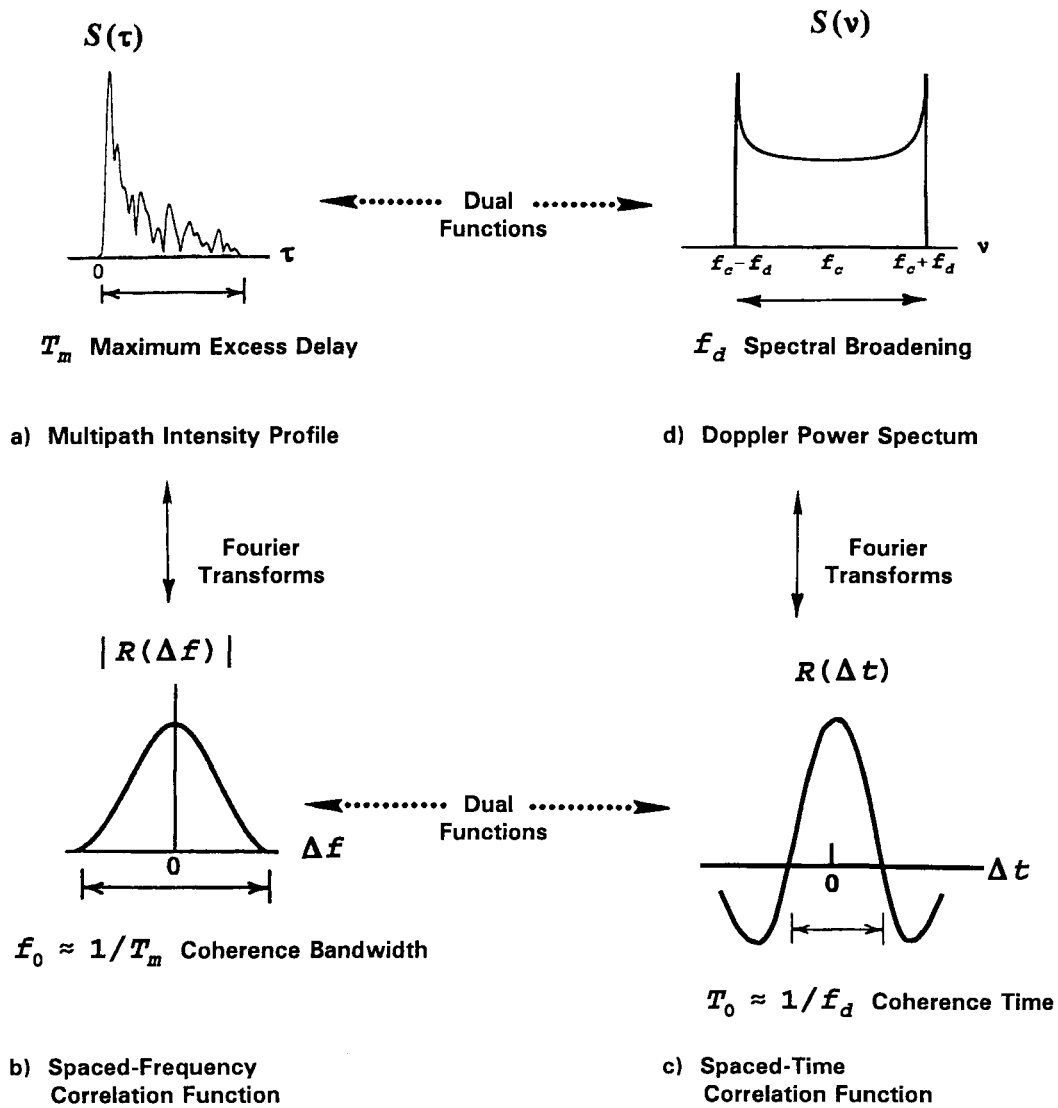


FIGURE 18.7: Relationships among the channel correlation functions and power density functions.

spectrum) need to be used [16]. For a single transmitted impulse, the time,  $T_m$ , between the first and last received component represents the **maximum excess delay**, during which the multipath signal power falls to some threshold level below that of the strongest component. The threshold level might be chosen at 10 dB or 20 dB below the level of the strongest component. Note, that for an ideal system (zero excess delay), the function  $S(\tau)$  would consist of an ideal impulse with weight equal to the total average received signal power.

### 18.4.1 Degradation Categories due to Signal Time-Spreading Viewed in the Time-Delay Domain

In a fading channel, the relationship between maximum excess delay time,  $T_m$ , and symbol time,  $T_s$ , can be viewed in terms of two different degradation categories, **frequency-selective fading** and **frequency nonselective** or **flat fading**, as indicated in Fig. 18.1, blocks 8 and 9, and Fig. 18.6. A channel is said to exhibit frequency-selective fading if  $T_m > T_s$ . This condition occurs whenever the received multipath components of a symbol extend beyond the symbol's time duration. Such multipath dispersion of the signal yields the same kind of ISI distortion that is caused by an electronic filter. In fact, another name for this category of fading degradation is **channel-induced ISI**. In the case of frequency-selective fading, mitigating the distortion is possible because many of the multipath components are resolvable by the receiver. Later, several such mitigation techniques are described.

A channel is said to exhibit frequency nonselective or flat fading if  $T_m < T_s$ . In this case, all of the received multipath components of a symbol arrive within the symbol time duration; hence, the components are not resolvable. Here, there is no channel-induced ISI distortion, since the signal time spreading does not result in significant overlap among neighboring received symbols. There is still performance degradation since the unresolvable phasor components can add up destructively to yield a substantial reduction in SNR. Also, signals that are classified as exhibiting flat fading can sometimes experience frequency-selective distortion. This will be explained later when viewing degradation in the frequency domain, where the phenomenon is more easily described. For loss in SNR due to flat fading, the mitigation technique called for is to improve the received SNR (or reduce the required SNR). For digital systems, introducing some form of signal diversity and using error-correction coding is the most efficient way to accomplish this.

## 18.5 Signal Time-Spreading Viewed in the Frequency Domain: Figure 18.1, Block 10—The Spaced-Frequency Correlation Function

---

A completely analogous characterization of signal dispersion can begin in the frequency domain. In Fig. 18.7(b), the function  $|R(\Delta f)|$  is seen, designated a **spaced-frequency correlation function**; it is the Fourier transform of  $S(\tau)$ .  $R(\Delta f)$  represents the correlation between the channel's response to two signals as a function of the frequency difference between the two signals. It can be thought of as the channel's frequency transfer function. Therefore, the time-spreading manifestation can be viewed as if it were the result of a filtering process. Knowledge of  $R(\Delta f)$  helps answer the question, "What is the correlation between received signals that are spaced in frequency  $\Delta f = f_1 - f_2$ ?"  $R(\Delta f)$  can be measured by transmitting a pair of sinusoids separated in frequency by  $\Delta f$ , cross-correlating the two separately received signals, and repeating the process many times with ever-larger separation  $\Delta f$ . Therefore, the measurement of  $R(\Delta f)$  can be made with a sinusoid that is swept in frequency across the band of interest (a wideband signal). The **coherence bandwidth**,  $f_0$ , is a statistical measure of the range of frequencies over which the channel passes all spectral components with approximately equal gain and linear phase. Thus, the coherence bandwidth represents a frequency range over which frequency components have a strong potential for amplitude correlation. That is, a signal's spectral components in that range are affected by the channel in a similar manner, as for example, exhibiting fading or no fading. Note that  $f_0$  and  $T_m$  are reciprocally related (within a multiplicative constant). As an approximation, it is possible to say that

$$f_0 \approx \frac{1}{T_m} \quad (18.8)$$

The maximum excess delay,  $T_m$ , is not necessarily the best indicator of how any given system will perform on a channel because different channels with the same value of  $T_m$  can exhibit very different profiles of signal intensity over the delay span. A more useful measurement of delay spread is most often characterized in terms of the root mean squared (rms) delay spread,  $\sigma_\tau$ , where

$$\sigma_\tau = \sqrt{\overline{\tau^2} - (\overline{\tau})^2} \quad (18.9)$$

$\overline{\tau}$  is the mean excess delay,  $(\overline{\tau})^2$  is the mean squared,  $\overline{\tau^2}$  is the second moment, and  $\sigma_\tau$  is the square root of the second central moment of  $S(\tau)$  [3].

An exact relationship between coherence bandwidth and delay spread does not exist, and must be derived from signal analysis (usually using Fourier techniques) of actual signal dispersion measurements in particular channels. Several approximate relationships have been described. If coherence bandwidth is defined as the frequency interval over which the channel's complex frequency transfer function has a correlation of at least 0.9, the coherence bandwidth is approximately [17]

$$f_0 \approx \frac{1}{50\sigma_\tau} \quad (18.10)$$

For the case of a mobile radio, an array of radially uniformly spaced scatterers, all with equal-magnitude reflection coefficients but independent, randomly occurring reflection phase angles [18, 19] is generally accepted as a useful model for urban surroundings. This model is referred to as the **dense-scatterer channel model**. With the use of such a model, coherence bandwidth has similarly been defined [18] for a bandwidth interval over which the channel's complex frequency transfer function has a correlation of at least 0.5 to be

$$f_0 = \frac{0.276}{\sigma_\tau} \quad (18.11)$$

The ionospheric-effects community employs the following definition

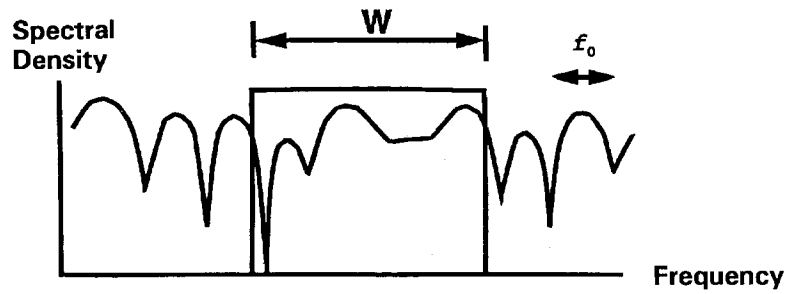
$$f_0 = \frac{1}{2\pi\sigma_\tau} \quad (18.12)$$

A more popular approximation of  $f_0$  corresponding to a bandwidth interval having a correlation of at least 0.5 is [3]

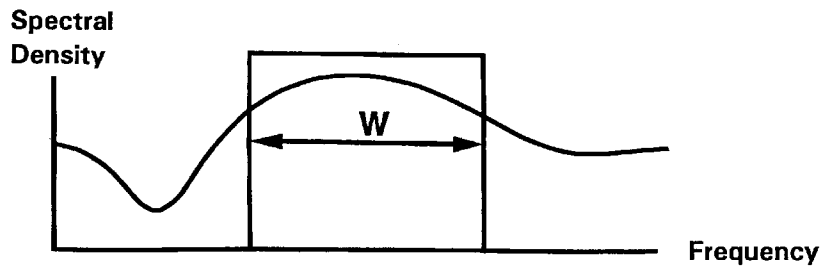
$$f_0 \approx \frac{1}{5\sigma_\tau} \quad (18.13)$$

### 18.5.1 Degradation Categories due to Signal Time-Spreading Viewed in the Frequency Domain

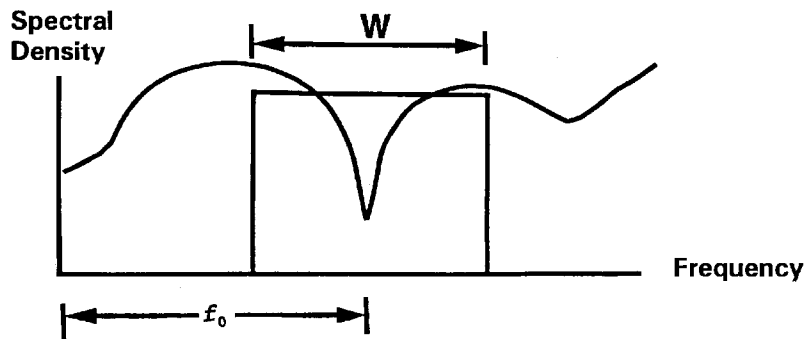
A channel is referred to as frequency-selective if  $f_0 < 1/T_s \approx W$ , where the symbol rate  $1/T_s$  is nominally taken to be equal to the signal bandwidth  $W$ . In practice,  $W$  may differ from  $1/T_s$  due to system filtering or data modulation type (quaternary phase shift keying, QPSK, minimum shift keying, MSK, etc.) [21]. Frequency-selective fading distortion occurs whenever a signal's spectral components are not all affected equally by the channel. Some of the signal's spectral components, falling outside the coherence bandwidth, will be affected differently (independently) compared to those components contained within the coherence bandwidth. This occurs whenever  $f_0 < W$  and is illustrated in Fig. 18.8(a).



(a) Typical Frequency-Selective Fading Case ( $f_0 < W$ )



(b) Typical Flat-Fading case ( $f_0 > W$ )



(c) Null of Channel Frequency-Transfer Function occurs at Signal Band Center ( $f_0 > W$ )

FIGURE 18.8: Relationships between the channel frequency-transfer function and a signal with bandwidth  $W$ .

Frequency-nonselctive or flat fading degradation occurs whenever  $f_0 > W$ . Hence, all of the signal's spectral components will be affected by the channel in a similar manner (e.g., fading or no fading); this is illustrated in Fig. 18.8(b). Flat-fading does not introduce channel-induced ISI distortion, but performance degradation can still be expected due to the loss in SNR whenever the signal is fading. In order to avoid channel-induced ISI distortion, the channel is required to exhibit flat fading by insuring that

$$f_0 > W \approx \frac{1}{T_s} \quad (18.14)$$

Hence, the channel coherence bandwidth  $f_0$  sets an upper limit on the transmission rate that can be used without incorporating an equalizer in the receiver.

For the flat-fading case, where  $f_0 > W$  (or  $T_m < T_s$ ), Fig. 18.8(b) shows the usual flat-fading pictorial representation. However, as a mobile radio changes its position, there will be times when the received signal experiences frequency-selective distortion even though  $f_0 > W$ . This is seen in Fig. 18.8(c), where the null of the channel's frequency transfer function occurs at the center of the signal band. Whenever this occurs, the baseband pulse will be especially mutilated by deprivation of its DC component. One consequence of the loss of DC (zero mean value) is the absence of a reliable pulse peak on which to establish the timing synchronization, or from which to sample the carrier phase carried by the pulse [18]. Thus, even though a channel is categorized as flat fading (based on rms relationships), it can still manifest frequency-selective fading on occasions. It is fair to say that a mobile radio channel, classified as having flat-fading degradation, cannot exhibit flat fading all of the time. As  $f_0$  becomes much larger than  $W$  (or  $T_m$  becomes much smaller than  $T_s$ ), less time will be spent in conditions approximating Fig. 18.8(c). By comparison, it should be clear that in Fig. 18.8(a) the fading is independent of the position of the signal band, and frequency-selective fading occurs all the time, not just occasionally.

## 18.6 Typical Examples of Flat Fading and Frequency-Selective Fading Manifestations

Figure 18.9 shows some examples of flat fading and frequency-selective fading for a direct-sequence spread-spectrum (DS/SS) system [20, 22]. In Fig. 18.9, there are three plots of the output of a pseudonoise (PN) code correlator vs. delay as a function of time (transmission or observation time). Each amplitude vs. delay plot is akin to  $S(\tau)$  vs.  $\tau$  shown in Fig. 18.7(a). The key difference is that the amplitudes shown in Fig. 18.9 represent the output of a correlator; hence, the waveshapes are a function not only of the impulse response of the channel, but also of the impulse response of the correlator. The delay time is expressed in units of chip durations (chips), where the chip is defined as the spread-spectrum minimal-duration keying element. For each plot, the observation time is shown on an axis perpendicular to the amplitude vs. time-delay plane. Figure 18.9 is drawn from a satellite-to-ground communications link exhibiting scintillation because of atmospheric disturbances. However, Fig. 18.9 is still a useful illustration of three different channel conditions that might apply to a mobile radio situation. A mobile radio that moves along the observation-time axis is affected by changing multipath profiles along the route, as seen in the figure. The scale along the observation-time axis is also in units of chips. In Fig. 18.9(a), the signal dispersion (one "finger" of return) is on the order of a chip time duration,  $T_{ch}$ . In a typical DS/SS system, the spread-spectrum signal bandwidth is approximately equal to  $1/T_{ch}$ ; hence, the normalized coherence bandwidth  $f_0 T_{ch}$  of approximately unity in Fig. 18.9(a) implies that the coherence bandwidth is about equal to the spread-spectrum bandwidth. This describes a channel that can be called frequency-nonselctive or slightly frequency-selective. In Fig. 18.9(b), where  $f_0 T_{ch} = 0.25$ , the signal dispersion is more pronounced. There is

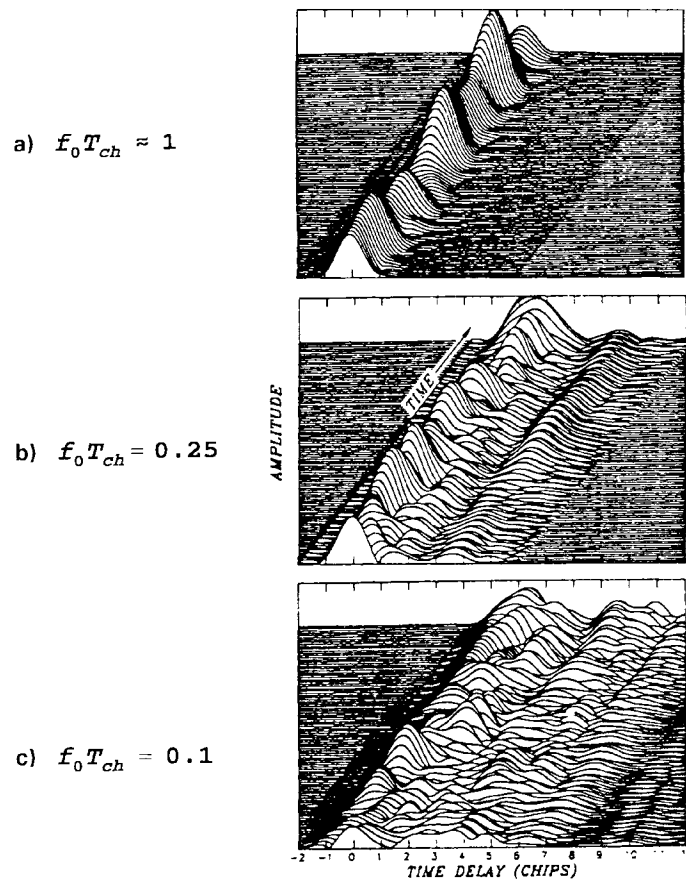


FIGURE 18.9: DS/SS Matched-filter output time-history examples for three levels of channel conditions, where  $T_{ch}$  is the time duration of a chip.

definite interchip interference, and the coherence bandwidth is approximately equal to 25% of the spread-spectrum bandwidth. In Fig. 18.9(c), where  $f_0 T_{ch} = 0.1$ , the signal dispersion is even more pronounced, with greater interchip-interference effects, and the coherence bandwidth is approximately equal to 10% of the spread-spectrum bandwidth. The channels of Figs. 18.9(b) and (c) can be categorized as moderately and highly frequency-selective, respectively, with respect to the basic signalling element, the chip. Later, we show that a DS/SS system operating over a frequency-selective channel at the chip level does not necessarily experience frequency-selective distortion at the symbol level.

## 18.7 Time Variance Viewed in the Time Domain: Figure 18.1, Block 13—The Spaced-Time Correlation Function

---

Until now, we have described signal dispersion and coherence bandwidth, parameters that describe the channel's time-spreading properties in a local area. However, they do not offer information about the time-varying nature of the channel caused by relative motion between a transmitter and receiver, or by movement of objects within the channel. For mobile-radio applications, the channel is time variant because motion between the transmitter and receiver results in propagation-path changes. Thus, for a transmitted continuous wave (CW) signal, as a result of such motion, the radio receiver sees variations in the signal's amplitude and phase. Assuming that all scatterers making up the channel are stationary, then whenever motion ceases, the amplitude and phase of the received signal remain constant; that is, the channel appears to be time invariant. Whenever motion begins again, the channel appears time variant. Since the channel characteristics are dependent on the positions of the transmitter and receiver, time variance in this case is equivalent to spatial variance.

Figure 18.7(c) shows the function  $R(\Delta t)$ , designated the **spaced-time correlation function**; it is the autocorrelation function of the channel's response to a sinusoid. This function specifies the extent to which there is correlation between the channel's response to a sinusoid sent at time  $t_1$  and the response to a similar sinusoid sent at time  $t_2$ , where  $\Delta t = t_2 - t_1$ . The **coherence time**,  $T_0$ , is a measure of the expected time duration over which the channel's response is essentially invariant. Earlier, we made measurements of signal dispersion and coherence bandwidth by using wideband signals. Now, to measure the time-variant nature of the channel, we use a narrowband signal. To measure  $R(\Delta t)$  we can transmit a single sinusoid ( $\Delta f = 0$ ) and determine the autocorrelation function of the received signal. The function  $R(\Delta t)$  and the parameter  $T_0$  provide us with knowledge about the fading rapidity of the channel. Note that for an ideal **time-invariant channel** (e.g., a mobile radio exhibiting no motion at all), the channel's response would be highly correlated for all values of  $\Delta t$ , and  $R(\Delta t)$  would be a constant function. When using the dense-scatterer channel model described earlier, with constant velocity of motion, and an unmodulated CW signal, the normalized  $R(\Delta t)$  is described as

$$R(\Delta t) = J_0(kV\Delta t) \quad (18.15)$$

where  $J_0(\cdot)$  is the zero-order Bessel function of the first kind,  $V$  is velocity,  $V\Delta t$  is distance traversed, and  $k = 2\pi/\lambda$  is the free-space phase constant (transforming distance to radians of phase). Coherence time can be measured in terms of either time or distance traversed (assuming some fixed velocity of motion). Amoroso described such a measurement using a CW signal and a dense-scatterer channel model [18]. He measured the statistical correlation between the combination of received magnitude and phase sampled at a particular antenna location  $x_0$ , and the corresponding combination sampled at some displaced location  $x_0 + \zeta$ , with displacement measured in units of wavelength  $\lambda$ . For a displacement  $\zeta$  of  $0.38\lambda$  between two antenna locations, the combined magnitudes and phases of the received CW are statistically uncorrelated. In other words, the state of the signal at  $x_0$  says nothing about the state of the signal at  $x_0 + \zeta$ . For a given velocity of motion, this displacement is readily transformed into units of time (coherence time).

### 18.7.1 The Concept of Duality

Two operators (functions, elements, or systems) are dual when the behavior of one with reference to a time-related domain (time or time-delay) is identical to the behavior of the other with reference to the corresponding frequency-related domain (frequency or Doppler shift).

In Fig. 18.7, we can identify functions that exhibit similar behavior across domains. For understanding the fading channel model, it is useful to refer to such functions as duals. For example,  $R(\Delta f)$  in Fig. 18.7(b), characterizing signal dispersion in the frequency domain, yields knowledge about the range of frequency over which two spectral components of a received signal have a strong potential for amplitude and phase correlation.  $R(\Delta t)$  in Fig. 18.7(c), characterizing fading rapidity in the time domain, yields knowledge about the span of time over which two received signals have a strong potential for amplitude and phase correlation. We have labeled these two correlation functions as duals. This is also noted in Fig. 18.1 as the duality between blocks 10 and 13, and in Fig. 18.6 as the duality between the time-spreading mechanism in the frequency domain and the time-variant mechanism in the time domain.

### 18.7.2 Degradation Categories due to Time Variance Viewed in the Time Domain

The time-variant nature of the channel or fading rapidity mechanism can be viewed in terms of two degradation categories as listed in Fig. 18.6: **fast fading** and **slow fading**. The terminology “fast fading” is used for describing channels in which  $T_0 < T_s$ , where  $T_0$  is the channel coherence time and  $T_s$  is the time duration of a transmission symbol. Fast fading describes a condition where the time duration in which the channel behaves in a correlated manner is short compared to the time duration of a symbol. Therefore, it can be expected that the fading character of the channel will change several times during the time that a symbol is propagating, leading to distortion of the baseband pulse shape. Analogous to the distortion previously described as channel-induced ISI, here distortion takes place because the received signal’s components are not all highly correlated throughout time. Hence, fast fading can cause the baseband pulse to be distorted, resulting in a loss of SNR that often yields an irreducible error rate. Such distorted pulses cause synchronization problems (failure of phase-locked-loop receivers), in addition to difficulties in adequately defining a matched filter.

A channel is generally referred to as introducing slow fading if  $T_0 > T_s$ . Here, the time duration that the channel behaves in a correlated manner is long compared to the time duration of a transmission symbol. Thus, one can expect the channel state to virtually remain unchanged during the time in which a symbol is transmitted. The propagating symbols will likely not suffer from the pulse distortion described above. The primary degradation in a slow-fading channel, as with flat fading, is loss in SNR.

## 18.8 Time Variance Viewed in the Doppler-Shift Domain: Figure 18.1, Block 16—The Doppler Power Spectrum

A completely analogous characterization of the time-variant nature of the channel can begin in the Doppler-shift (frequency) domain. Figure 18.7(d) shows a **Doppler power spectral density**,  $S(v)$ , plotted as a function of Doppler-frequency shift,  $v$ . For the case of the dense-scatterer model, a vertical receive antenna with constant azimuthal gain, a uniform distribution of signals arriving at all arrival angles throughout the range  $(0, 2\pi)$ , and an unmodulated CW signal, the signal spectrum at the antenna terminals is [19]

$$S(v) = \frac{1}{\pi f_d \sqrt{1 - \left(\frac{v - f_c}{f_d}\right)^2}} \quad (18.16)$$

The equality holds for frequency shifts of  $\nu$  that are in the range  $\pm f_d$  about the carrier frequency  $f_c$  and would be zero outside that range. The shape of the RF Doppler spectrum described by Eq. (18.16) is classically bowl-shaped, as seen in Fig. 18.7(d). Note that the spectral shape is a result of the dense-scatterer channel model. Equation (18.16) has been shown to match experimental data gathered for mobile radio channels [23]; however, different applications yield different spectral shapes. For example, the dense-scatterer model does not hold for the indoor radio channel; the channel model for an indoor area assumes  $S(\nu)$  to be a flat spectrum [24].

In Fig. 18.7(d), the sharpness and steepness of the boundaries of the Doppler spectrum are due to the sharp upper limit on the Doppler shift produced by a vehicular antenna traveling among the stationary scatterers of the dense scatterer model. The largest magnitude (infinite) of  $S(\nu)$  occurs when the scatterer is directly ahead of the moving antenna platform or directly behind it. In that case the magnitude of the frequency shift is given by

$$f_d = \frac{V}{\lambda} \quad (18.17)$$

where  $V$  is relative velocity and  $\lambda$  is the signal wavelength.  $f_d$  is positive when the transmitter and receiver move toward each other and negative when moving away from each other. For scatterers directly broadside of the moving platform, the magnitude of the frequency shift is zero. The fact that Doppler components arriving at exactly  $0^\circ$  and  $180^\circ$  have an infinite power spectral density is not a problem, since the angle of arrival is continuously distributed and the probability of components arriving at exactly these angles is zero [3, 19].

$S(\nu)$  is the Fourier transform of  $R(\Delta t)$ . We know that the Fourier transform of the autocorrelation function of a time series is the magnitude squared of the Fourier transform of the original time series. Therefore, measurements can be made by simply transmitting a sinusoid (narrowband signal) and using Fourier analysis to generate the power spectrum of the received amplitude [16]. This Doppler power spectrum of the channel yields knowledge about the spectral spreading of a transmitted sinusoid (impulse in frequency) in the Doppler-shift domain. As indicated in Fig. 18.7,  $S(\nu)$  can be regarded as the dual of the multipath intensity profile,  $S(\tau)$ , since the latter yields knowledge about the time spreading of a transmitted impulse in the time-delay domain. This is also noted in Fig. 18.1 as the duality between blocks 7 and 16, and in Fig. 18.6 as the duality between the time-spreading mechanism in the time-delay domain and the time-variant mechanism in the Doppler-shift domain.

Knowledge of  $S(\nu)$  allows us to glean how much spectral broadening is imposed on the signal as a function of the rate of change in the channel state. The width of the Doppler power spectrum is referred to as the **spectral broadening** or **Doppler spread**, denoted by  $f_d$ , and sometimes called the **fading bandwidth** of the channel. Equation (18.16) describes the Doppler frequency shift. In a typical multipath environment, the received signal arrives from several reflected paths with different path distances and different angles of arrival, and the Doppler shift of each arriving path is generally different from that of another path. The effect on the received signal is seen as a Doppler spreading or spectral broadening of the transmitted signal frequency, rather than a shift. Note that the Doppler spread,  $f_d$ , and the coherence time,  $T_0$ , are reciprocally related (within a multiplicative constant). Therefore, we show the approximate relationship between the two parameters as

$$T_0 \approx \frac{1}{f_d} \quad (18.18)$$

Hence, the Doppler spread  $f_d$  or  $1/T_0$  is regarded as the typical **fading rate** of the channel. Earlier,  $T_0$  was described as the expected time duration over which the channel's response to a sinusoid is essentially invariant. When  $T_0$  is defined more precisely as the time duration over which the

channel's response to a sinusoid has a correlation of at least 0.5, the relationship between  $T_0$  and  $f_d$  is approximately [4]

$$T_0 \approx \frac{9}{16\pi f_d} \quad (18.19)$$

A popular “rule of thumb” is to define  $T_0$  as the geometric mean of Eqs. (18.18) and (18.19). This yields

$$T_0 = \sqrt{\frac{9}{16\pi f_d^2}} = \frac{0.423}{f_d} \quad (18.20)$$

For the case of a 900 MHz mobile radio, Fig. 18.10 illustrates the typical effect of Rayleigh fading on a signal's envelope amplitude vs. time [3]. The figure shows that the distance traveled by the

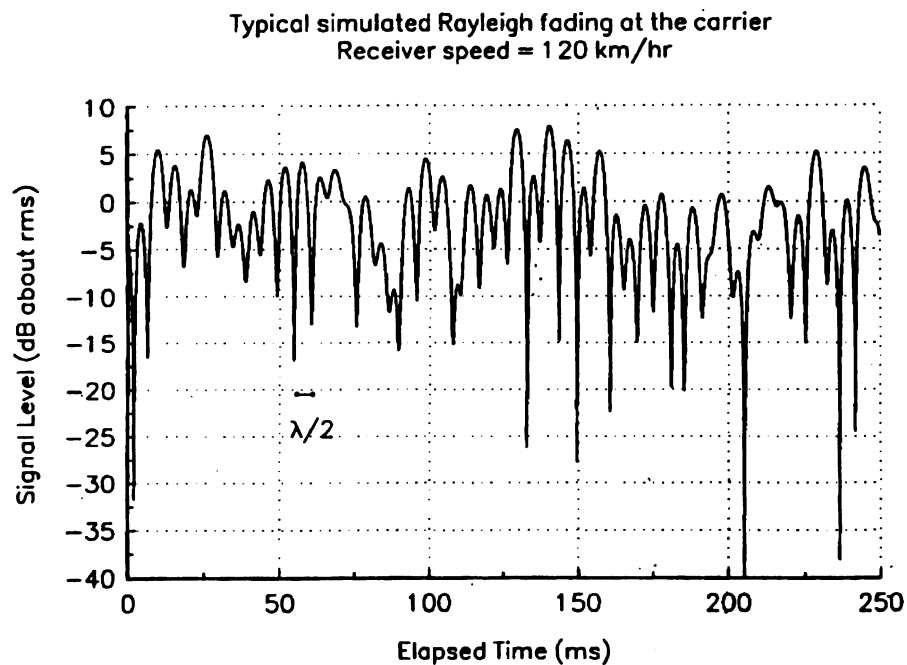


FIGURE 18.10: A typical Rayleigh fading envelope at 900 MHz.

mobile in the time interval corresponding to two adjacent nulls (small-scale fades) is on the order of a half-wavelength ( $\lambda/2$ ) [3]. Thus, from Fig. 18.10 and Eq. (18.17), the time (approximately, the coherence time) required to traverse a distance  $\lambda/2$  when traveling at a constant velocity,  $V$ , is:

$$T_0 \approx \frac{\lambda/2}{V} = \frac{0.5}{f_d} \quad (18.21)$$

Thus, when the interval between fades is taken to be  $\lambda/2$ , as in Fig. 18.10, the resulting expression for  $T_0$  in Eq. (18.21) is quite close to the rule-of-thumb shown in Eq. (18.20). Using Eq. (18.21), with the parameters shown in Fig. 18.10 (velocity = 120 km/hr, and carrier frequency = 900 MHz), it is

straightforward to compute that the coherence time is approximately 5 ms and the Doppler spread (channel fading rate) is approximately 100 Hz. Therefore, if this example represents a voice-grade channel with a typical transmission rate of  $10^4$  symbols/s, the fading rate is considerably less than the symbol rate. Under such conditions, the channel would manifest slow-fading effects. Note that if the abscissa of Fig. 18.10 were labeled in units of wavelength instead of time, the figure would look the same for any radio frequency and any antenna speed.

## 18.9 Analogy Between Spectral Broadening in Fading Channels and Spectral Broadening in Digital Signal Keying

---

Help is often needed in understanding why spectral broadening of the signal is a function of fading rate of the channel. Figure 18.11 uses the keying of a digital signal (such as amplitude-shift-keying or frequency-shift-keying) to illustrate an analogous case. Figure 18.11(a) shows that a single tone,  $\cos 2\pi f_c t$  ( $-\infty < t < \infty$ ) that exists for all time is characterized in the frequency domain in terms of impulses (at  $\pm f_c$ ). This frequency domain representation is ideal (i.e., zero bandwidth), since the tone is pure and neverending. In practical applications, digital signalling involves switching (keying) signals on and off at a required rate. The keying operation can be viewed as multiplying the infinite-duration tone in Fig. 18.11(a) by an ideal rectangular (switching) function in Fig. 18.11(b). The frequency-domain description of the ideal rectangular function is of the form  $(\sin f)/f$ . In Fig. 18.11(c), the result of the multiplication yields a tone,  $\cos 2\pi f_c t$ , that is time-duration limited in the interval  $-T/2 < t < T/2$ . The resulting spectrum is obtained by convolving the spectral impulses in part (a) with the  $(\sin f)/f$  function in part (b), yielding the broadened spectrum in part (c). It is further seen that, if the signalling occurs at a faster rate characterized by the rectangle of shorter duration in part (d), the resulting spectrum of the signal in part (e) exhibits greater spectral broadening. The changing state of a fading channel is somewhat analogous to the keying on and off of digital signals. The channel behaves like a switch, turning the signal “on” and “off.” The greater the rapidity of the change in the channel state, the greater the spectral broadening of the received signals. The analogy is not exact because the on and off switching of signals may result in phase discontinuities, but the typical multipath-scatterer environment induces phase-continuous effects.

## 18.10 Degradation Categories due to Time Variance, Viewed in the Doppler-Shift Domain

---

A channel is referred to as fast fading if the symbol rate,  $1/T_s$  (approximately equal to the signalling rate or bandwidth  $W$ ) is less than the fading rate,  $1/T_0$  (approximately equal to  $f_d$ ); that is, fast fading is characterized by

$$W < f_d \quad (18.22a)$$

or

$$T_s > T_0 \quad (18.22b)$$

Conversely, a channel is referred to as slow fading if the signalling rate is greater than the fading

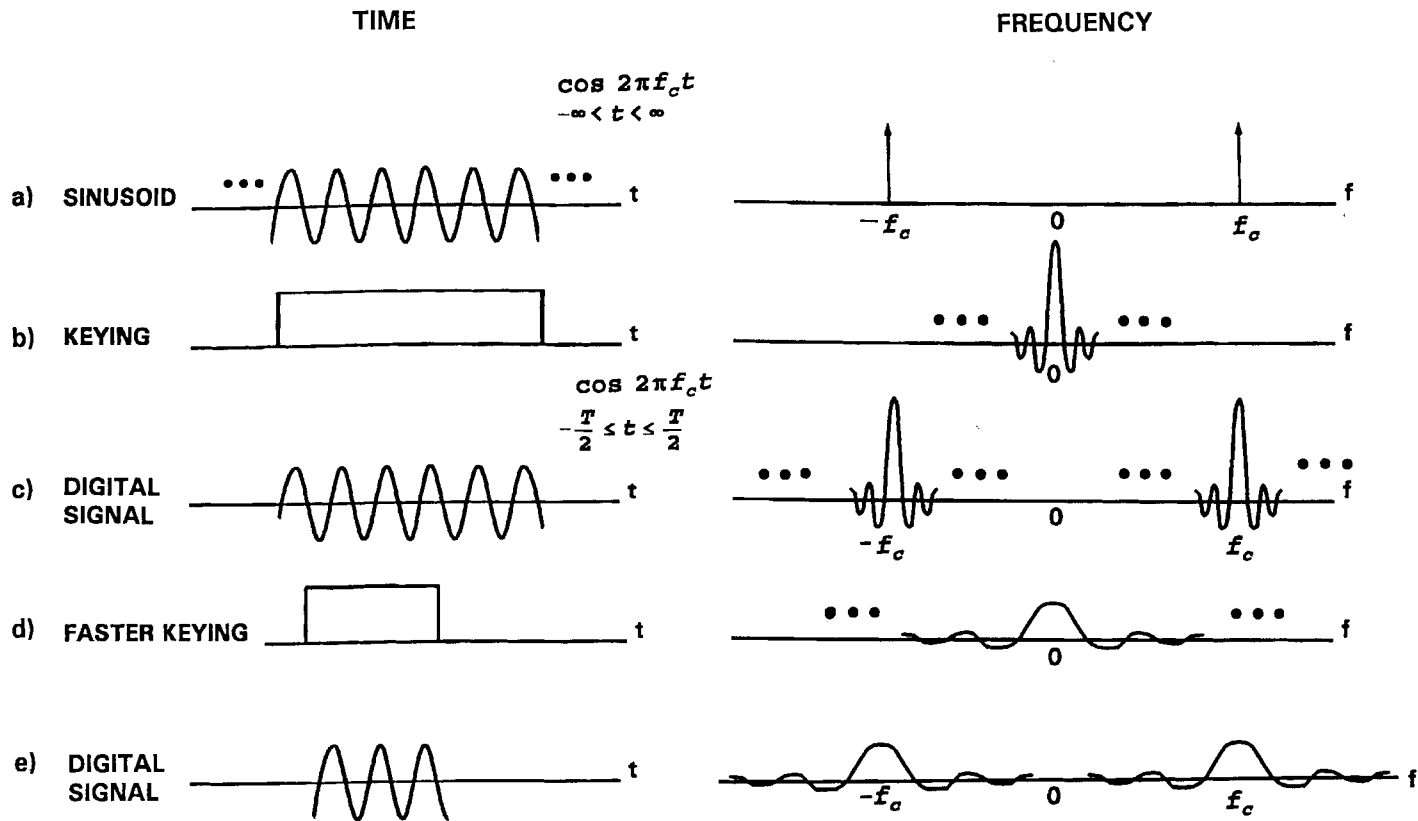


FIGURE 18.11: Analogy between spectral broadening in fading and spectral broadening in keying a digital signal.

rate. Thus, in order to avoid signal distortion caused by fast fading, the channel must be made to exhibit slow fading by insuring that the signalling rate must exceed the channel fading rate. That is

$$W > f_d \quad (18.23a)$$

or

$$T_s < T_0 \quad (18.23b)$$

In Eq. (18.14), it was shown that due to signal dispersion, the coherence bandwidth,  $f_0$ , sets an upper limit on the signalling rate which can be used without suffering frequency-selective distortion. Similarly, Eq. (18.23a–18.23b) shows that due to Doppler spreading, the channel fading rate,  $f_d$ , sets a lower limit on the signalling rate that can be used without suffering fast-fading distortion. For HF communicating systems, when teletype or Morse-coded messages were transmitted at a low data rate, the channels were often fast fading. However, most present-day terrestrial mobile-radio channels can generally be characterized as slow fading.

Equation (18.23a–18.23b) doesn't go far enough in describing what we desire of the channel. A better way to state the requirement for mitigating the effects of fast fading would be that we desire  $W \gg f_d$  (or  $T_s \ll T_0$ ). If this condition is not satisfied, the random frequency modulation (FM) due to varying Doppler shifts will limit the system performance significantly. The Doppler effect yields an irreducible error rate that cannot be overcome by simply increasing  $E_b/N_0$  [25]. This irreducible error rate is most pronounced for any modulation that involves switching the carrier phase. A single specular Doppler path, without scatterers, registers an instantaneous frequency shift, classically calculated as  $f_d = V/\lambda$ . However, a combination of specular and multipath components yields a rather complex time dependence of instantaneous frequency which can cause much larger frequency swings than  $\pm V/\lambda$  when detected by an instantaneous frequency detector (a nonlinear device) [26]. Ideally, coherent demodulators that lock onto and track the information signal should suppress the effect of this FM noise and thus cancel the impact of Doppler shift. However, for large values of  $f_d$ , carrier recovery becomes a problem because very wideband (relative to the data rate) phase-lock loops (PLLs) need to be designed. For voice-grade applications with bit-error rates of  $10^{-3}$  to  $10^{-4}$ , a large value of Doppler shift is considered to be on the order of  $0.01 \times W$ . Therefore, to avoid fast-fading distortion and the Doppler-induced irreducible error rate, the signalling rate should exceed the fading rate by a factor of 100 to 200 [27]. The exact factor depends on the signal modulation, receiver design, and required error-rate [3], [26]–[29]. Davarian [29] showed that a frequency-tracking loop can help lower, but not completely remove, the irreducible error rate in a mobile system when using differential minimum-shift keyed (DMSK) modulation.

## 18.11 Mitigation Methods

---

Figure 18.12, subtitled “The Good, The Bad, and The Awful,” highlights three major performance categories in terms of bit-error probability,  $P_B$ , vs.  $E_b/N_0$ . The leftmost exponentially-shaped curve represents the performance that can be expected when using any nominal modulation type in AWGN. Observe that with a reasonable amount of  $E_b/N_0$ , good performance results. The middle curve, referred to as the **Rayleigh limit**, shows the performance degradation resulting from a loss in SNR that is characteristic of flat fading or slow fading when there is no line-of-sight signal component present. The curve is a function of the reciprocal of  $E_b/N_0$  (an inverse-linear function), so for

reasonable values of SNR, performance will generally be “bad.” In the case of Rayleigh fading, parameters with overbars are often introduced to indicate that a mean is being taken over the “ups” and “downs” of the fading experience. Therefore, one often sees such bit-error probability plots with mean parameters denoted by  $\overline{P_B}$  and  $\overline{E_b/N_0}$ . The curve that reaches an irreducible level, sometimes called an **error floor**, represents “awful” performance, where the bit-error probability can approach the value of 0.5. This shows the severe distorting effects of frequency-selective fading or fast fading.

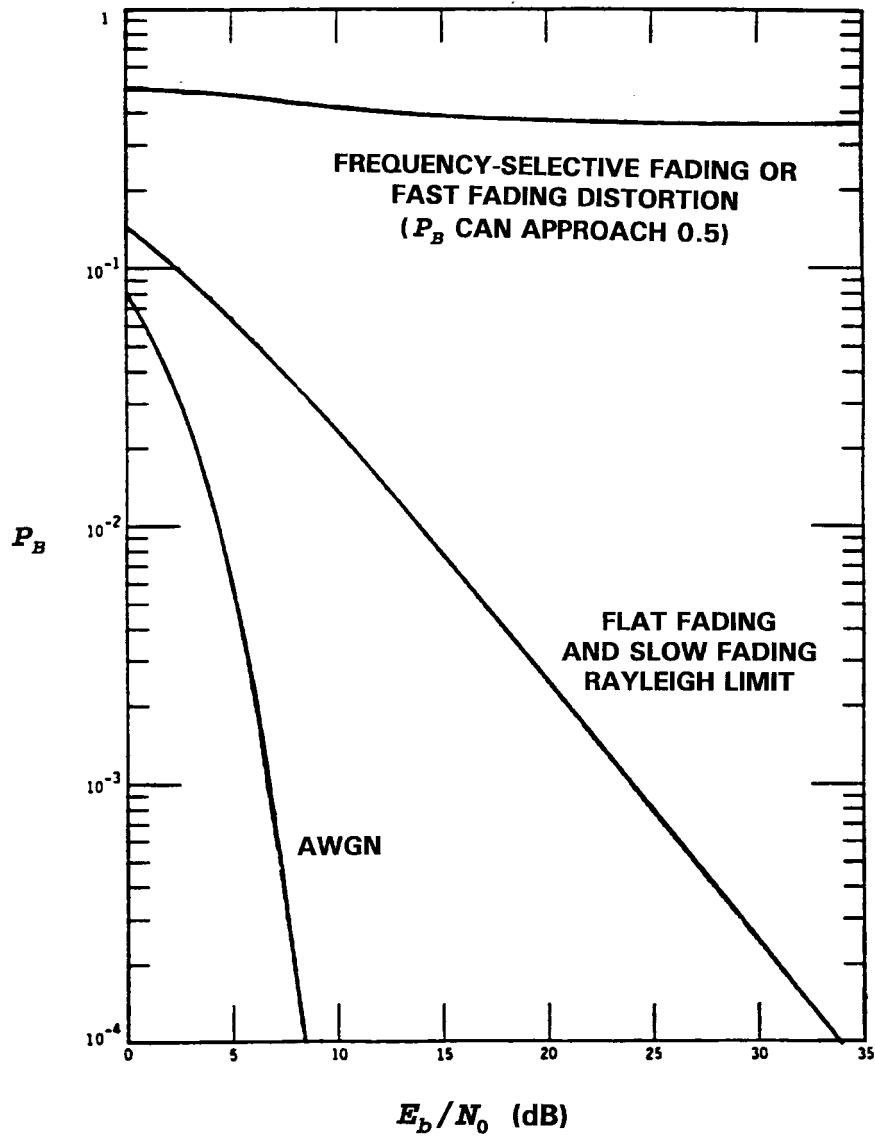


FIGURE 18.12: Error performance: The good, the bad, and the awful.

If the channel introduces signal distortion as a result of fading, the system performance can exhibit an irreducible error rate; when larger than the desired error rate, no amount of  $E_b/N_0$  will help achieve the desired level of performance. In such cases, the general approach for improving performance is to use some form of mitigation to remove or reduce the distortion. The mitigation method depends on whether the distortion is caused by frequency-selective fading or fast fading. Once the distortion has been mitigated, the  $P_B$  vs.  $E_b/N_0$  performance should have transitioned from the “awful” bottoming out curve to the merely “bad” Rayleigh limit curve. Next, we can further ameliorate the effects of fading and strive to approach AWGN performance by using some form of diversity to provide the receiver with a collection of uncorrelated samples of the signal, and by using a powerful error-correction code.

In Fig. 18.13, several mitigation techniques for combating the effects of both signal distortion and loss in SNR are listed. Just as Figs. 18.1 and 18.6 serve as a guide for characterizing fading phenomena and their effects, Fig. 18.13 can similarly serve to describe mitigation methods that can be used to ameliorate the effects of fading. The mitigation approach to be used should follow two basic steps: first, provide distortion mitigation; second, provide diversity.

### 18.11.1 Mitigation to Combat Frequency-Selective Distortion

- Equalization can compensate for the channel-induced ISI that is seen in frequency-selective fading. That is, it can help move the operating point from the error-performance curve that is “awful” in Fig. 18.12 to the one that is “bad.” The process of equalizing the ISI involves some method of gathering the dispersed symbol energy back together into its original time interval. In effect, equalization involves insertion of a filter to make the combination of channel and filter yield a flat response with linear phase. The phase linearity is achieved by making the equalizer filter the complex conjugate of the time reverse of the dispersed pulse [30]. Because in a mobile system the channel response varies with time, the equalizer filter must also change or adapt to the time-varying channel. Such equalizer filters are, therefore, called adaptive equalizers. An equalizer accomplishes more than distortion mitigation; it also provides diversity. Since distortion mitigation is achieved by gathering the dispersed symbol’s energy back into the symbol’s original time interval so that it doesn’t hamper the detection of other symbols, the equalizer is simultaneously providing each received symbol with energy that would otherwise be lost.
- The decision feedback equalizer (DFE) has a feedforward section that is a linear transversal filter [30] whose length and tap weights are selected to coherently combine virtually all of the current symbol’s energy. The DFE also has a feedback section which removes energy that remains from previously detected symbols [14], [30]–[32]. The basic idea behind the DFE is that once an information symbol has been detected, the ISI that it induces on future symbols can be estimated and subtracted before the detection of subsequent symbols.
- The maximum-likelihood sequence estimation (MLSE) equalizer tests all possible data sequences (rather than decoding each received symbol by itself) and chooses the data sequence that is the most probable of the candidates. The MLSE equalizer was first proposed by Forney [33] when he implemented the equalizer using the Viterbi decoding algorithm [34]. The MLSE is optimal in the sense that it minimizes the probability of a sequence error. Because the Viterbi decoding algorithm is the way in which the MLSE equalizer is typically implemented, the equalizer is often referred to as the **Viterbi equalizer**. Later in this chapter, we illustrate the adaptive equalization performed in the

### TO COMBAT DISTORTION

#### FREQ-SELECTIVE DISTORTION

- Adaptive Equalization (e.g., Decision Feedback, Viterbi Equalizer)
- Spread Spectrum — DS or FH
- Orthogonal FDM (OFDM)
- Pilot Signal

#### FAST-FADING DISTORTION

- Robust Modulation
- Signal Redundancy to increase Signaling Rate
- Coding & Interleaving

### TO COMBAT LOSS IN SNR

#### FLAT-FADING AND SLOW-FADING

- Some Type of Diversity to get Additional Uncorrelated Estimates of Signal
- Error-Correction Coding

#### DIVERSITY TYPES

- Time (e.g., Interleaving)
- Frequency (e.g., BW Expansion, Spread Spectrum FH or DS with Rake Receiver)
- Spatial (e.g., Spaced Receive Antennas)
- Polarization

FIGURE 18.13: Basic mitigation types.

Global System for Mobile Communications (GSM) using the Viterbi equalizer.

- Spread-spectrum techniques can be used to mitigate frequency-selective ISI distortion because the hallmark of any spread-spectrum system is its capability to reject interference, and ISI is a type of interference. Consider a direct-sequence spread-spectrum (DS/SS) binary phase shift keying (PSK) communication channel comprising one direct path and one reflected path. Assume that the propagation from transmitter to receiver results in a multipath wave that is delayed by  $\tau_k$  compared to the direct wave. If the receiver is synchronized to the waveform arriving via the direct path, the received signal,  $r(t)$ , neglecting noise, can be expressed as

$$r(t) = Ax(t)g(t) \cos(2\pi f_c t) + \alpha Ax(t - \tau_k)g(t - \tau_k) \cos(2\pi f_c t + \Theta) \quad (18.24)$$

where  $x(t)$  is the data signal,  $g(t)$  is the pseudonoise (PN) spreading code, and  $\tau_k$  is the differential time delay between the two paths. The angle  $\Theta$  is a random phase, assumed to be uniformly distributed in the range  $(0, 2\pi)$ , and  $\alpha$  is the attenuation of the multipath signal relative to the direct path signal. The receiver multiplies the incoming  $r(t)$  by the code  $g(t)$ . If the receiver is synchronized to the direct path signal, multiplication by the code signal yields

$$Ax(t)g^2(t) \cos(2\pi f_c t) + \alpha Ax(t - \tau_k)g(t)g(t - \tau_k) \cos(2\pi f_c t + \Theta) \quad (18.25)$$

where  $g^2(t) = 1$ , and if  $\tau_k$  is greater than the chip duration, then,

$$\left| \int g^*(t)g(t - \tau_k) dt \right| \ll \int g^*(t)g(t) dt \quad (18.26)$$

over some appropriate interval of integration (correlation), where  $*$  indicates complex conjugate, and  $\tau_k$  is equal to or larger than the PN chip duration. Thus, the spread spectrum system effectively eliminates the multipath interference by virtue of its code-correlation receiver. Even though channel-induced ISI is typically transparent to DS/SS systems, such systems suffer from the loss in energy contained in all the multipath components not seen by the receiver. The need to gather up this lost energy belonging to the received chip was the motivation for developing the Rake receiver [35]–[37]. The Rake receiver dedicates a separate correlator to each multipath component (finger). It is able to coherently add the energy from each finger by selectively delaying them (the earliest component gets the longest delay) so that they can all be coherently combined.

- Earlier, we described a channel that could be classified as flat fading, but occasionally exhibits frequency-selective distortion when the null of the channel's frequency transfer function occurs at the center of the signal band. The use of DS/SS is a good way to mitigate such distortion because the wideband SS signal would span many lobes of the selectively faded frequency response. Hence, a great deal of pulse energy would then be passed by the scatterer medium, in contrast to the nulling effect on a relatively narrowband signal [see Fig. 18.8(c)] [18].
- Frequency-hopping spread-spectrum (FH/SS) can be used to mitigate the distortion due to frequency-selective fading, provided the hopping rate is at least equal to the symbol rate. Compared to DS/SS, mitigation takes place through a different mechanism. FH receivers avoid multipath losses by rapid changes in the transmitter frequency band, thus avoiding the interference by changing the receiver band position before the arrival of the multipath signal.

- Orthogonal frequency-division multiplexing (OFDM) can be used in frequency-selective fading channels to avoid the use of an equalizer by lengthening the symbol duration. The signal band is partitioned into multiple subbands, each one exhibiting a lower symbol rate than the original band. The subbands are then transmitted on multiple orthogonal carriers. The goal is to reduce the symbol rate (signalling rate),  $W \approx 1/T_s$ , on each carrier to be less than the channel's coherence bandwidth  $f_0$ . OFDM was originally referred to as Kineplex. The technique has been implemented in the U.S. in mobile radio systems [38], and has been chosen by the European community under the name Coded OFDM (COFDM), for high-definition television (HDTV) broadcasting [39].
- Pilot signal is the name given to a signal intended to facilitate the coherent detection of waveforms. Pilot signals can be implemented in the frequency domain as an in-band tone [40], or in the time domain as a pilot sequence, which can also provide information about the channel state and thus improve performance in fading [41].

### 18.11.2 Mitigation to Combat Fast-Fading Distortion

- For fast fading distortion, use a robust modulation (noncoherent or differentially coherent) that does not require phase tracking, and reduce the detector integration time [20].
- Increase the symbol rate,  $W \approx 1/T_s$ , to be greater than the fading rate,  $f_d \approx 1/T_0$ , by adding signal redundancy.
- Error-correction coding and interleaving can provide mitigation because instead of providing more signal energy, a code reduces the required  $E_b/N_0$ . For a given  $E_b/N_0$ , with coding present, the error floor will be lowered compared to the uncoded case.
- An interesting filtering technique can provide mitigation in the event of fast-fading distortion and frequency-selective distortion occurring simultaneously. The frequency-selective distortion can be mitigated by the use of an OFDM signal set. Fast fading, however, will typically degrade conventional OFDM because the Doppler spreading corrupts the orthogonality of the OFDM subcarriers. A polyphase filtering technique [42] is used to provide time-domain shaping and duration extension to reduce the spectral sidelobes of the signal set and thus help preserve its orthogonality. The process introduces known ISI and adjacent channel interference (ACI) which are then removed by a post-processing equalizer and canceling filter [43].

### 18.11.3 Mitigation to Combat Loss in SNR

After implementing some form of mitigation to combat the possible distortion (frequency-selective or fast fading), the next step is to use some form of diversity to move the operating point from the error-performance curve labeled as “bad” in Fig. 18.12 to a curve that approaches AWGN performance. The term “diversity” is used to denote the various methods available for providing the receiver with uncorrelated renditions of the signal. Uncorrelated is the important feature here, since it would not help the receiver to have additional copies of the signal if the copies were all equally poor. Listed below are some of the ways in which diversity can be implemented.

- Time diversity—Transmit the signal on  $L$  different time slots with time separation of at least  $T_0$ . Interleaving, often used with error-correction coding, is a form of time diversity.
- Frequency diversity—Transmit the signal on  $L$  different carriers with frequency separation of at least  $f_0$ . Bandwidth expansion is a form of frequency diversity. The

signal bandwidth,  $W$ , is expanded to be greater than  $f_0$ , thus providing the receiver with several independently fading signal replicas. This achieves frequency diversity of the order  $L = W/f_0$ . Whenever  $W$  is made larger than  $f_0$ , there is the potential for frequency-selective distortion unless we further provide some mitigation such as equalization. Thus, an expanded bandwidth can improve system performance (via diversity) only if the frequency-selective distortion the diversity may have introduced is mitigated.

- Spread spectrum is a form of bandwidth expansion that excels at rejecting interfering signals. In the case of direct-sequence spread-spectrum (DS/SS), it was shown earlier that multipath components are rejected if they are delayed by more than one chip duration. However, in order to approach AWGN performance, it is necessary to compensate for the loss in energy contained in those rejected components. The Rake receiver (described later) makes it possible to coherently combine the energy from each of the multipath components arriving along different paths. Thus, used with a Rake receiver, DS/SS modulation can be said to achieve path diversity. The Rake receiver is needed in phase-coherent reception, but in differentially coherent bit detection, a simple delay line (one bit long) with complex conjugation will do the trick [44].
- Frequency-hopping spread-spectrum (FH/SS) is sometimes used as a diversity mechanism. The GSM system uses slow FH (217 hops/s) to compensate for those cases where the mobile user is moving very slowly (or not at all) and happens to be in a spectral null.
- Spatial diversity is usually accomplished through the use of multiple receive antennas, separated by a distance of at least 10 wavelengths for a base station (much less for a mobile station). Signal processing must be employed to choose the best antenna output or to coherently combine all the outputs. Systems have also been implemented with multiple spaced transmitters; an example is the Global Positioning System (GPS).
- Polarization diversity [45] is yet another way to achieve additional uncorrelated samples of the signal.
- Any diversity scheme may be viewed as a trivial form of repetition coding in space or time. However, there exist techniques for improving the loss in SNR in a fading channel that are more efficient and more powerful than repetition coding. Error-correction coding represents a unique mitigation technique, because instead of providing more signal energy it reduces the required  $E_b/N_0$  in order to accomplish the desired error performance. Error-correction coding coupled with interleaving [20], [46]–[51] is probably the most prevalent of the mitigation schemes used to provide improved performance in a fading environment.

## 18.12 Summary of the Key Parameters Characterizing Fading Channels

---

We summarize the conditions that must be met so that the channel does not introduce frequency-selective distortion and fast-fading distortion. Combining the inequalities of Eqs. (18.14) and (18.23a–18.23b), we obtain

$$f_0 > W > f_d \quad (18.27a)$$

or

$$T_m < T_s < T_0 \quad (18.27b)$$

In other words, we want the channel coherence bandwidth to exceed our signalling rate, which in turn should exceed the fading rate of the channel. Recall that without distortion mitigation,  $f_0$  sets an upper limit on signalling rate, and  $f_d$  sets a lower limit on it.

### 18.12.1 Fast-Fading Distortion: Example #1

If the inequalities of Eq. (18.27a–18.27b) are not met and distortion mitigation is not provided, distortion will result. Consider the fast-fading case where the signalling rate is less than the channel fading rate, that is,

$$f_0 > W < f_d \quad (18.28)$$

Mitigation consists of using one or more of the following methods. (See Fig. 18.13).

- Choose a modulation/demodulation technique that is most robust under fast-fading conditions. That means, for example, avoiding carrier recovery with PLLs since the fast fading could keep a PLL from achieving lock conditions.
- Incorporate sufficient redundancy so that the transmission symbol rate exceeds the channel fading rate. As long as the transmission symbol rate does not exceed the coherence bandwidth, the channel can be classified as flat fading. However, even flat-fading channels will experience frequency-selective distortion whenever a channel null appears at the band center.

Since this happens only occasionally, mitigation might be accomplished by adequate error-correction coding and interleaving.

- The above two mitigation approaches should result in the demodulator operating at the Rayleigh limit [20] (see Fig. 18.12). However, there may be an irreducible floor in the error-performance vs.  $E_b/N_0$  curve due to the FM noise that results from the random Doppler spreading. The use of an in-band pilot tone and a frequency-control loop can lower this irreducible performance level.
- To avoid this error floor caused by random Doppler spreading, increase the signalling rate above the fading rate still further ( $100\text{--}200 \times$  fading rate) [27]. This is one architectural motive behind time-division multiple access (TDMA) mobile systems.
- Incorporate error-correction coding and interleaving to lower the floor and approach AWGN performance.

### 18.12.2 Frequency-Selective Fading Distortion: Example #2

Consider the frequency-selective case where the coherence bandwidth is less than the symbol rate; that is,

$$f_0 < W > f_d \quad (18.29)$$

Mitigation consists of using one or more of the following methods. (See Fig. 18.13).

- Since the transmission symbol rate exceeds the channel-fading rate, there is no fast-fading distortion. Mitigation of frequency-selective effects is necessary. One or more of the following techniques may be considered:

- Adaptive equalization, spread spectrum (DS or FH), OFDM, pilot signal. The European GSM system uses a midamble training sequence in each transmission time slot so that the receiver can learn the impulse response of the channel. It then uses a Viterbi equalizer (explained later) for mitigating the frequency-selective distortion.
- Once the distortion effects have been reduced, introduce some form of diversity and error-correction coding and interleaving in order to approach AWGN performance. For direct-sequence spread-spectrum (DS/SS) signalling, the use of a Rake receiver (explained later) may be used for providing diversity by coherently combining multipath components that would otherwise be lost.

### 18.12.3 Fast-Fading and Frequency-Selective Fading Distortion: Example #3

Consider the case where the coherence bandwidth is less than the signalling rate, which in turn is less than the fading rate. The channel exhibits both fast-fading and frequency-selective fading which is expressed as

$$f_0 < W < f_d \quad (18.30a)$$

or

$$f_0 < f_d \quad (18.30b)$$

Recalling from Eq. (18.27a–18.27b) that  $f_0$  sets an upper limit on signalling rate and  $f_d$  sets a lower limit on it, this is a difficult design problem because, unless distortion mitigation is provided, the maximum allowable signalling rate is (in the strict terms of the above discussion) less than the minimum allowable signalling rate. Mitigation in this case is similar to the initial approach outlined in example #1.

- Choose a modulation/demodulation technique that is most robust under fast-fading conditions.
- Use transmission redundancy in order to increase the transmitted symbol rate.
- Provide some form of frequency-selective mitigation in a manner similar to that outlined in example #2.
- Once the distortion effects have been reduced, introduce some form of diversity and error-correction coding and interleaving in order to approach AWGN performance.

## 18.13 The Viterbi Equalizer as Applied to GSM

---

Figure 18.14 shows the GSM time-division multiple access (TDMA) frame, having a duration of 4.615 ms and comprising 8 slots, one assigned to each active mobile user. A normal transmission burst occupying one slot of time contains 57 message bits on each side of a 26-bit midamble called a **training** or **sounding sequence**. The slot-time duration is 0.577 ms (or the slot rate is 1733 slots/s). The purpose of the midamble is to assist the receiver in estimating the impulse response of the channel in an adaptive way (during the time duration of each 0.577 ms slot). In order for the technique to be effective, the fading behavior of the channel should not change appreciably during the time interval

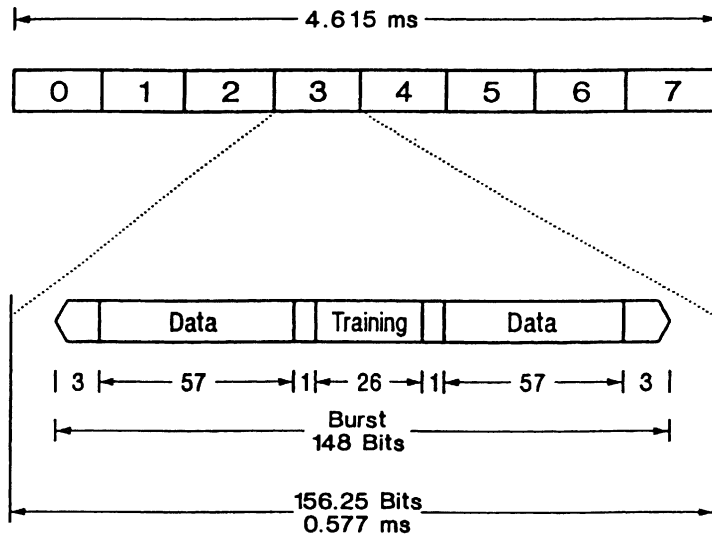


FIGURE 18.14: The GSM TDMA frame and time-slot containing a normal burst.

of one slot. In other words, there should not be any fast-fading degradation during a slot time when the receiver is using knowledge from the midamble to compensate for the channel's fading behavior. Consider the example of a GSM receiver used aboard a high-speed train, traveling at a constant velocity of 200 km/hr (55.56 m/s). Assume the carrier frequency to be 900 MHz, (the wavelength is  $\lambda = 0.33$  m). From Eq. (18.21), we can calculate that a half-wavelength is traversed in approximately the time (coherence time)

$$T_0 \approx \frac{\lambda/2}{V} \approx 3 \text{ ms} \quad (18.31)$$

Therefore, the channel coherence time is over 5 times greater than the slot time of 0.577 ms. The time needed for a significant change in fading behavior is relatively long compared to the time duration of one slot. Note, that the choices made in the design of the GSM TDMA slot time and midamble were undoubtedly influenced by the need to preclude fast fading with respect to a slot-time duration, as in this example.

The GSM symbol rate (or bit rate, since the modulation is binary) is 271 kilosymbols/s and the bandwidth is  $W = 200$  kHz. If we consider that the typical rms delay spread in an urban environment is on the order of  $\sigma_\tau = 2\mu\text{s}$ , then using Eq. (18.13) the resulting coherence bandwidth is  $f_0 \approx 100$  kHz. It should therefore be apparent that since  $f_0 < W$ , the GSM receiver must utilize some form of mitigation to combat frequency-selective distortion. To accomplish this goal, the Viterbi equalizer is typically implemented.

Figure 18.15 illustrates the basic functional blocks used in a GSM receiver for estimating the channel impulse response, which is then used to provide the detector with channel-corrected reference waveforms [52]. In the final step, the Viterbi algorithm is used to compute the MLSE of the message. As stated in Eq. (18.2), a received signal can be described in terms of the transmitted signal convolved with the impulse response of the channel,  $h_c(t)$ . We show this below, using the notation of a received training sequence,  $r_{tr}(t)$ , and the transmitted training sequence,  $s_{tr}(t)$ , as follows:

$$r_{tr}(t) = s_{tr}(t) * h_c(t) \quad (18.32)$$

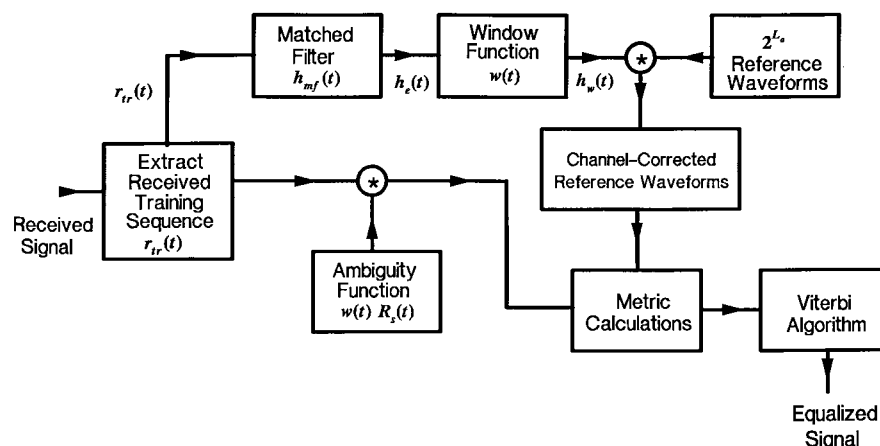


FIGURE 18.15: The Viterbi equalizer as applied to GSM.

where  $*$  denotes convolution. At the receiver,  $r_{tr}(t)$  is extracted from the normal burst and sent to a filter having impulse response,  $h_{mf}(t)$ , that is matched to  $s_{tr}(t)$ . This matched filter yields at its output an estimate of  $h_c(t)$ , denoted  $h_e(t)$ , developed from Eq. (18.32) as follows.

$$\begin{aligned}
 h_e(t) &= r_{tr}(t) * h_{mf}(t) \\
 &= s_{tr}(t) * h_c(t) * h_{mf}(t) \\
 &= R_s(t) * h_c(t)
 \end{aligned}
 \tag{18.33}$$

where  $R_s(t)$  is the autocorrelation function of  $s_{tr}(t)$ . If  $R_s(t)$  is a highly peaked (impulse-like) function, then  $h_e(t) \approx h_c(t)$ .

Next, using a windowing function,  $w(t)$ , we truncate  $h_e(t)$  to form a computationally affordable function,  $h_w(t)$ . The window length must be large enough to compensate for the effect of typical channel-induced ISI. The required observation interval  $L_0$  for the window can be expressed as the sum of two contributions. The interval of length  $L_{CISI}$  is due to the controlled ISI caused by Gaussian filtering of the baseband pulses, which are then MSK modulated. The interval of length  $L_C$  is due to the channel-induced ISI caused by multipath propagation; therefore,  $L_0$  can be written as

$$L_0 = L_{CISI} + L_C \tag{18.34}$$

The GSM system is required to provide mitigation for distortion due to signal dispersions of approximately 15–20  $\mu s$ . The bit duration is 3.69  $\mu s$ . Thus, the Viterbi equalizer used in GSM has a memory of 4–6 bit intervals. For each  $L_0$ -bit interval in the message, the function of the Viterbi equalizer is to find the most likely  $L_0$ -bit sequence out of the  $2^{L_0}$  possible sequences that might have been transmitted. Determining the most likely  $L_0$ -bit sequence requires that  $2^{L_0}$  meaningful reference waveforms be created by modifying (or disturbing) the  $2^{L_0}$  ideal waveforms in the same way that the channel has disturbed the transmitted message. Therefore, the  $2^{L_0}$  reference waveforms are convolved with the windowed estimate of the channel impulse response,  $h_w(t)$  in order to derive the disturbed or channel-corrected reference waveforms. Next, the channel-corrected reference waveforms are compared against the received data waveforms to yield metric calculations. However, before the comparison takes place, the received data waveforms are convolved with the known windowed autocorrelation function  $w(t)R_s(t)$ , transforming them in a manner comparable to that applied to the

reference waveforms. This filtered message signal is compared to all possible  $2^{L_0}$  channel-corrected reference signals, and metrics are computed as required by the Viterbi decoding algorithm (VDA). The VDA yields the maximum likelihood estimate of the transmitted sequence [34].

## 18.14 The Rake Receiver Applied to Direct-Sequence Spread-Spectrum (DS/SS) Systems

---

Interim Specification 95 (IS-95) describes a DS/SS cellular system that uses a Rake receiver [35]–[37] to provide path diversity. In Fig. 18.16, five instances of chip transmissions corresponding to the code sequence 1 0 1 1 1 are shown, with the transmission or observation times labeled  $t_{-4}$  for the earliest transmission and  $t_0$  for the latest. Each abscissa shows three “fingers” of a signal that arrive at the receiver with delay times  $\tau_1$ ,  $\tau_2$ , and  $\tau_3$ . Assume that the intervals between the  $t_i$  transmission times and the intervals between the  $\tau_i$  delay times are each one chip long. From this, one can conclude that the finger arriving at the receiver at time  $t_{-4}$ , with delay  $\tau_3$ , is time coincident with two other fingers, namely the fingers arriving at times  $t_{-3}$  and  $t_{-2}$  with delays  $\tau_2$  and  $\tau_1$ , respectively. Since, in this example, the delayed components are separated by exactly one chip time, they are *just* resolvable. At the receiver, there must be a sounding device that is dedicated to estimating the  $\tau_i$  delay times. Note that for a terrestrial mobile radio system, the fading rate is relatively slow (milliseconds) or the channel coherence time large compared to the chip time ( $T_0 > T_{ch}$ ). Hence, the changes in  $\tau_i$  occur slowly enough so that the receiver can readily adapt to them.

Once the  $\tau_i$  delays are estimated, a separate correlator is dedicated to processing each finger. In this example, there would be three such dedicated correlators, each one processing a delayed version of the same chip sequence 1 0 1 1 1. In Fig. 18.16, each correlator receives chips with power profiles represented by the sequence of fingers shown along a diagonal line. Each correlator attempts to match these arriving chips with the same PN code, similarly delayed in time. At the end of a symbol interval (typically there may be hundreds or thousands of chips per symbol), the outputs of the correlators are coherently combined, and a symbol detection is made. At the chip level, the Rake receiver resembles an equalizer, but its real function is to provide diversity.

The interference-suppression nature of DS/SS systems stems from the fact that a code sequence arriving at the receiver merely one chip time late, will be approximately orthogonal to the particular PN code with which the sequence is correlated. Therefore, any code chips that are delayed by one or more chip times will be suppressed by the correlator. The delayed chips only contribute to raising the noise floor (correlation sidelobes). The mitigation provided by the Rake receiver can be termed path diversity, since it allows the energy of a chip that arrives via multiple paths to be combined coherently. Without the Rake receiver, this energy would be transparent and therefore lost to the DS/SS system. In Fig. 18.16, looking vertically above point  $\tau_3$ , it is clear that there is interchip interference due to different fingers arriving simultaneously. The spread-spectrum processing gain allows the system to endure such interference at the chip level. No other equalization is deemed necessary in IS-95.

## 18.15 Conclusion

---

In this chapter, the major elements that contribute to fading in a communication channel have been characterized. Figure 18.1 was presented as a guide for the characterization of fading phenomena. Two types of fading, large-scale and small-scale, were described. Two manifestations of small-scale fading (signal dispersion and fading rapidity) were examined, and the examination involved two views, time and frequency. Two degradation categories were defined for dispersion: frequency-selective

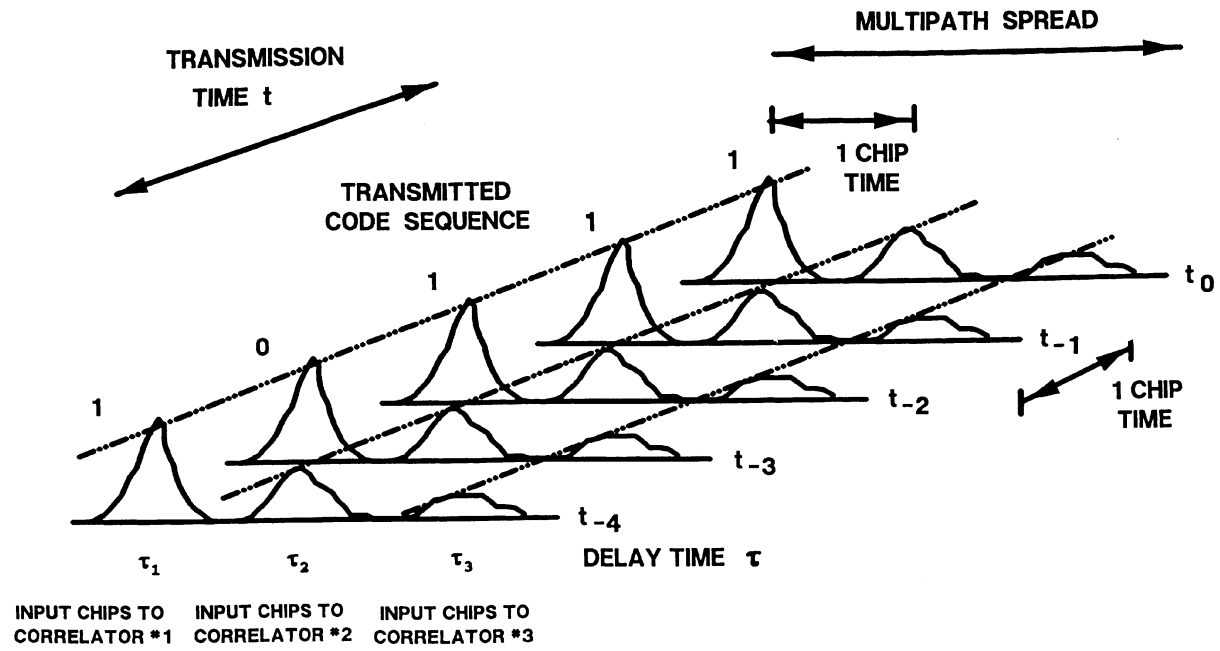


FIGURE 18.16: Example of received chips seen by a 3-finger rake receiver.

fading and flat-fading. Two degradation categories were defined for fading rapidity: fast and slow. The small-scale fading degradation categories were summarized in Fig. 18.6. A mathematical model using correlation and power density functions was presented in Fig. 18.7. This model yields a nice symmetry, a kind of “poetry” to help us view the Fourier transform and duality relationships that describe the fading phenomena. Further, mitigation techniques for ameliorating the effects of each degradation category were treated, and these techniques were summarized in Fig. 18.13. Finally, mitigation methods that have been implemented in two system types, GSM and CDMA systems meeting IS-95, were described.

## References

---

- [1] Sklar, B., *Digital Communications: Fundamentals and Applications*, Prentice-Hall, Englewood Cliffs, NJ, Ch. 4, 1988.
- [2] Van Trees, H.L., *Detection, Estimation, and Modulation Theory, Part I*, John Wiley & Sons, New York, Ch. 4, 1968.
- [3] Rappaport, T.S., *Wireless Communications*, Prentice-Hall, Upper Saddle River, New Jersey, Chs. 3 and 4, 1996.
- [4] Greenwood, D. and Hanzo, L., Characterisation of Mobile Radio Channels, *Mobile Radio Communications*, Steele, R., Ed., Pentech Press, London, Ch. 2, 1994.
- [5] Lee, W.C.Y., Elements of cellular mobile radio systems, *IEEE Trans. Vehicular Technol.*, V-35(2), 48–56, May 1986.
- [6] Okumura, Y. et al., Field strength and its variability in VHF and UHF land mobile radio service, *Rev. Elec. Comm. Lab.*, 16(9-10), 825–873, 1968.
- [7] Hata, M., Empirical formulæ for propagation loss in land mobile radio services, *IEEE Trans. Vehicular Technol.*, VT-29(3), 317–325, 1980.
- [8] Seidel, S.Y. et al., Path loss, scattering and multipath delay statistics in four European cities for digital cellular and microcellular radiotelephone, *IEEE Trans. Vehicular Technol.*, 40(4), 721–730, Nov. 1991.
- [9] Cox, D.C., Murray, R., and Norris, A., 800 MHz Attenuation measured in and around suburban houses, *AT&T Bell Laboratory Technical Journal*, 673(6), 921–954, Jul.-Aug. 1984.
- [10] Schilling, D.L. et al., Broadband CDMA for personal communications systems, *IEEE Commun. Mag.*, 29(11), 86–93, Nov. 1991.
- [11] Andersen, J.B., Rappaport, T.S., and Yoshida, S., Propagation measurements and models for wireless communications channels, *IEEE Commun. Mag.*, 33(1), 42–49, Jan. 1995.
- [12] Amoroso, F., Investigation of signal variance, bit error rates and pulse dispersion for DSPN signalling in a mobile dense scatterer ray tracing model, *Intl. J. Satellite Commun.*, 12, 579–588, 1994.
- [13] Bello, P.A., Characterization of randomly time-variant linear channels, *IEEE Trans. Commun. Syst.*, 360–393, Dec. 1963.
- [14] Proakis, J.G., *Digital Communications*, McGraw-Hill, New York, Ch. 7, 1983.
- [15] Green, P.E., Jr., Radar astronomy measurement techniques, *MIT Lincoln Laboratory*, Lexington, MA, Tech. Report No. 282, Dec. 1962.
- [16] Pahlavan, K. and Levesque, A.H., *Wireless Information Networks*, John Wiley & Sons, New York, Chs. 3 and 4, 1995.
- [17] Lee, W.Y.C., *Mobile Cellular Communications*, McGraw-Hill, New York, 1989.
- [18] Amoroso, F., Use of DS/SS signalling to mitigate Rayleigh fading in a dense scatterer environment, *IEEE Personal Commun.*, 3(2), 52–61, Apr. 1996.

- [19] Clarke, R.H., A statistical theory of mobile radio reception, *Bell Syst. Tech. J.*, 47(6), 957–1000, Jul.-Aug. 1968.
- [20] Bogusch, R.L., *Digital Communications in Fading Channels: Modulation and Coding*, Mission Research Corp., Santa Barbara, California, Report No. MRC-R-1043, Mar. 11, 1987.
- [21] Amoroso, F., The bandwidth of digital data signals, *IEEE Commun. Mag.*, 18(6), 13–24, Nov. 1980.
- [22] Bogusch, R.L. et al., Frequency selective propagation effects on spread-spectrum receiver tracking, *Proc. IEEE*, 69(7), 787–796, Jul. 1981.
- [23] Jakes, W.C., Ed., *Microwave Mobile Communications*, John Wiley & Sons, New York, 1974.
- [24] *Joint Technical Committee of Committee T1 R1P1.4 and TIA TR46.3.3/TR45.4.4 on Wireless Access*, Draft Final Report on RF Channel Characterization, Paper No. JTC(AIR)/94.01.17-238R4, Jan. 17, 1994.
- [25] Bello, P.A. and Nelin, B.D., The influence of fading spectrum on the binary error probabilities of incoherent and differentially coherent matched filter receivers, *IRE Trans. Commun. Syst.*, CS-10, 160–168, Jun. 1962.
- [26] Amoroso, F., Instantaneous frequency effects in a Doppler scattering environment, *IEEE International Conference on Communications*, 1458–1466, Jun. 7–10, 1987.
- [27] Bateman, A.J. and McGeehan, J.P., Data transmission over UHF fading mobile radio channels, *IEEE Proc.*, 131, Pt. F(4), 364–374, Jul. 1984.
- [28] Feher, K., *Wireless Digital Communications*, Prentice-Hall, Upper Saddle River, NJ, 1995.
- [29] Davarian, F., Simon, M., and Sumida, J., DMSK: A Practical 2400-bps Receiver for the Mobile Satellite Service, Jet Propulsion Laboratory Publication 85-51 (MSAT-X Report No. 111), Jun. 15, 1985.
- [30] Rappaport, T.S., *Wireless Communications*, Prentice-Hall, Upper Saddle River, NJ, Ch. 6, 1996.
- [31] Bogusch, R.L., Guigliano, F.W., and Knepp, D.L., Frequency-selective scintillation effects and decision feedback equalization in high data-rate satellite links, *Proc. IEEE*, 71(6), 754–767, Jun. 1983.
- [32] Qureshi, S.U.H., Adaptive equalization, *Proc. IEEE*, 73(9), 1340–1387, Sept. 1985.
- [33] Forney, G.D., The Viterbi algorithm, *Proc. IEEE*, 61(3), 268–278, Mar. 1978.
- [34] Sklar, B., *Digital Communications: Fundamentals and Applications*, Prentice-Hall, Englewood Cliffs, NJ, Ch. 6, 1988.
- [35] Price, R. and Green, P.E., Jr., A communication technique for multipath channels, *Proc. IRE*, 555–570, Mar. 1958.
- [36] Turin, G.L., Introduction to spread-spectrum antimultipath techniques and their application to urban digital radio, *Proc. IEEE*, 68(3), 328–353, Mar. 1980.
- [37] Simon, M.K., Omura, J.K., Scholtz, R.A., and Levitt, B.K., *Spread Spectrum Communications Handbook*, McGraw-Hill, New York, 1994.
- [38] Birchler, M.A. and Jasper, S.C., A 64 kbps Digital Land Mobile Radio System Employing M-16QAM, *Proceedings of the 1992 IEEE Intl. Conference on Selected Topics in Wireless Communications*, Vancouver, British Columbia, 158–162, Jun. 25–26, 1992.
- [39] Sari, H., Karam, G., and Jeanclaude, I., Transmission techniques for digital terrestrial TV broadcasting, *IEEE Commun. Mag.*, 33(2), 100–109, Feb. 1995.
- [40] Cavers, J.K., The performance of phase locked transparent tone-in-band with symmetric phase detection, *IEEE Trans. Commun.*, 39(9), 1389–1399, Sept. 1991.
- [41] Moher, M.L. and Lodge, J.H., TCMP—A modulation and coding strategy for Rician fading channel, *IEEE J. Selected Areas Commun.*, 7(9), 1347–1355, Dec. 1989.

- [42] Harris, F., On the Relationship Between Multirate Polyphase FIR Filters and Windowed, Overlapped FFT Processing, *Proceedings of the Twenty Third Annual Asilomar Conference on Signals, Systems, and Computers*, Pacific Grove, California, 485–488, Oct. 30 to Nov. 1, 1989.
- [43] Lowdermilk, R.W. and Harris, F., Design and Performance of Fading Insensitive Orthogonal Frequency Division Multiplexing (OFDM) using Polyphase Filtering Techniques, *Proceedings of the Thirtieth Annual Asilomar Conference on Signals, Systems, and Computers*, Pacific Grove, California, Nov. 3–6, 1996.
- [44] Kavehrad, M. and Bodeep, G.E., Design and experimental results for a direct-sequence spread-spectrum radio using differential phase-shift keying modulation for indoor wireless communications, *IEEE JSAC*, SAC-5(5), 815–823, Jun. 1987.
- [45] Hess, G.C., *Land-Mobile Radio System Engineering*, Artech House, Boston, 1993.
- [46] Hagenauer, J. and Lutz, E., Forward error correction coding for fading compensation in mobile satellite channels, *IEEE JSAC*, SAC-5(2), 215–225, Feb. 1987.
- [47] McLane, P.I. et al., PSK and DPSK trellis codes for fast fading, shadowed mobile satellite communication channels, *IEEE Trans. Commun.*, 36(11), 1242–1246, Nov. 1988.
- [48] Schlegel, C. and Costello, D.J., Jr., Bandwidth efficient coding for fading channels: code construction and performance analysis, *IEEE JSAC*, 7(9), 1356–1368, Dec. 1989.
- [49] Edbauer, F., Performance of interleaved trellis-coded differential 8-PSK modulation over fading channels, *IEEE J. Selected Areas Commun.*, 7(9), 1340–1346, Dec. 1989.
- [50] Soliman, S. and Mokrani, K., Performance of coded systems over fading dispersive channels, *IEEE Trans. Commun.*, 40(1), 51–59, Jan. 1992.
- [51] Divsalar, D. and Pollara, F., Turbo Codes for PCS Applications, *Proc. ICC'95*, Seattle, Washington, 54–59, Jun. 18–22, 1995.
- [52] Hanzo, L. and Stefanov, J., The Pan-European Digital Cellular Mobile Radio System—known as GSM, *Mobile Radio Communications*. Steele, R., Ed., Pentech Press, London, Ch. 8, 1992.